Journal of the Meteorological Society of Japan, Vol.79, No.5, pp.999–1033, 2001

A Mesoscale Model Intercomparison: A Case of Explosive Development of a Tropical Cyclone (COMPARE III)

By Masashi Nagata

Japan Meteorological Agency, Tokyo, Japan

Lance Leslie

University of New South Wales, Sydney, Australia

Hirotaka Kamahori

Meteorological Research Institute, JMA, Tsukuba, Japan

Ryoichi Nomura, Hiroshi Mino

Japan Meteorological Agency, Tokyo, Japan

Yoshio Kurihara

Frontier Research System for Global Change, Tokyo, Japan

Eric Rogers

National Centers for Environmental Prediction, NOAA, Camp Springs MD, USA

Russell L. Elsberry

Naval Postgraduate School, Monterey CA, USA

B. K. Basu

National Centre for Medium Range Weather Forecasting, New Delhi, India

Andrea Buzzi

ISAO–CNR, Bologna, Italy

Javier Calvo

Instituto Nacional de Meteorologia, Madrid, Spain

Michel Desgagné

Recherche en Prévision Numérique, Environment Canada, Dorval, Quebec, Canada

Massimo D'Isidoro

ISAO–CNR, Bologna, Italy

Song-You Hong[1]

National Centers for Environmental Prediction, NOAA, Camp Springs MD, USA

Jack Katzfey

Commonwealth Scientific and Industrial Research Organisation, Melbourne, Australia

Detlev Majewski

Deutscher Wetterdienst, Offenbach, Germany

Piero Malguzzi

ISAO-CNR, Bologna, Italy

John McGregor

Commonwealth Scientific and Industrial Research Organisation, Melbourne, Australia

Akihiko Murata

Meteorological Research Institute, JMA, Tsukuba, Japan

Jason Nachamkin

Naval Research Laboratory, Monterey CA, USA

Michel Roch

Recherche en Prévision Numérique, Environment Canada, Dorval, Quebec, Canada

and

Clive Wilson

The Meteorological Office, Bracknell, Berkshire, UK

(Manuscript received 25 October 2000, in revised form 15 June 2001)

Abstract

The performance of current mesoscale numerical models is evaluated in a case of model intercomparison project (COMPARE III). Explosive development of Typhoon Flo (9019) occurred in the case in September 1990 during the cooperative three field experiments, ESCAP/WMO-led SPECTRUM, US-led TCM-90, and former USSR-led TYPHOON-90 in the western North Pacific. Sensitivity to initial fields as well as impact of enhanced horizontal resolution are examined in the model intercomparison.

Both track and intensity predictions are very sensitive to the choice of initial fields prepared with different data assimilation systems and the use of a particular synthetic tropical cyclone vortex. Horizontal resolution enhanced from 50 km through 20 km down to a 10 km grid has a large impact on intensity prediction. This is presumably due to a better presentation of inner structure with higher resolution. There is little impact on track prediction in this target period when the typhoon was in its before-recurvature stage. While most models show large biases in underestimating central pressure deepening, some of the participating models with a particular initial field succeed in reproducing qualitatively the time evolution of central pressure, including slow deepening in the first half and rapid deepening in the second half of the simulation period of 72 hours. However, differences leading to different intensity predictions among models have yet to be identified. Intercomparison of the simulation results shows that wind field has a close relationship with precipitation distribution. This suggests that better prediction of precipitation distribution is crucial for better prediction of wind field, and vice versa.

Corresponding author: Masashi Nagata, National Typhoon Center, Forecast Division, Japan Meteorological Agency, Ote-machi 1-3-4, Chiyoda-ku, Tokyo 100-8122, Japan.
E-mail: mnagata@met.kishou.go.jp

1 Present affiliation: Yonsei University, Seoul, Korea.

Through the COMPARE III experiments, it has become clear that precise simulation of tropical cyclone structure, especially in the inner-core region, is very important for accurate intensity prediction. Consideration, therefore, should be given to this point, when improvements in resolution, initialization, and physics of numerical models for tropical cyclone intensity prediction are reviewed.

1. Introduction

Numerical models have been improved significantly to produce tropical cyclone (TC) track predictions with steadily increasing accuracy. According to the policy statement of the American Meteorological Society on Hurricane Research and Forecasting (adopted by AMS Council on 14 February 2000)*, NOAA National Hurricane Center (NHC)'s TC track forecast errors for the decade 1989–1998 averaged 87, 162, 301, and 449 km for the Atlantic 12-, 24-, 48-, and 72-h forecasts, respectively. The Japan Meteorological Agency (JMA)'s TC track forecast errors averaged for the last four years (1997–2000) were 161, 299, and 427 km for the western North Pacific 24-, 48-, and 72-h forecasts, respectively, according to the Regional Specialized Meteorological Center (RSMC) Tokyo–Typhoon Center's Annual Report on its activities for the 2000 season. These good forecasts owe much to enhanced numerical model predictions. Recently, in one case of Hurricane Andrew, Liu et al. (1997) demonstrated that a high-resolution, non-hydrostatic model with hybrid-type physics (combined cumulus parameterization and explicit microphysics) was capable of simulating realistically not only the very low central pressure and strong winds, but also the structure of the intense hurricane, even in the inner-core region.

Current operational numerical TC prediction models, however, still have considerable mean absolute errors (or root-mean-square errors), and occasionally large misses in intensity predictions. Even the GFDL Hurricane Model (Kurihara et al. 1993), for instance, which is known as the best performer among operational limited-area TC prediction models, has average prediction errors of maximum wind speed of 6.1, 7.9, 8.4, and 9.7 $m\,s^{-1}$ for 12-, 24-, 48-, and 72-h forecasts, respectively, for the TCs in the Atlantic in 1995 (Kurihara et al. 1998), and those of 10.6, 11.2, 11.9 $m\,s^{-1}$ for 24-, 48-, and 72-h forecasts, respectively for 125 TC cases in the western North Pacific in 1995 (Wu et al. 2000). Its performance in Atlantic TC intensity prediction is still much (slightly) worse in short (long) forecast hours than a statistical scheme (Kurihara et al. 1998), although it shows modest skill.

While TC motion (track) will still remain a major target of the development of numerical prediction models (Elsberry 1995), the authors believe that TC intensity can also become an increasingly feasible target for numerical prediction models of higher resolutions, with carefully prepared initial conditions in the next decade. This outlook is supported by the fact that another tropical cyclone prediction model, besides the GFDL model, showed some capability in TC intensity predictions (Nagata et al. 1998; Nagata and Mino 2000; Mino and Nagata 2001). It is, therefore, worthwhile to explore the capability of current state-of-the-art mesoscale models in the simulation and prediction of TC intensity evolutions. For this exploration, we took the opportunity of Case III of the Comparison of Mesoscale Prediction and Research Experiments (COMPARE) project under the World Meteorological Organization (WMO)—Commission for Atmospheric Research (CAS)/WCRP—Joint Scientific Committee (JSC)—Working Group for Numerical Experimentation (WGNE). The reader is referred to Gyakum et al. (1996) for the three long-term objectives of the COMPARE project.

An event of explosive tropical cyclone development has been chosen for the intercomparison experiment, whose major findings are presented in this paper. The purpose of this research is, therefore, to identify and then address, if possible, important scientific issues relating to the understanding and prediction of explosive development of tropical cyclones. The event occurred during the three cooperative field experiments for tropical cyclone research conducted in August and September 1990: the Special Experiment concerning Typhoon Recurvature and Unusual Movement (SPECTRUM), Tropical Cyclone Motion–90 (TCM–90) (Elsberry 1990; Elsberry et al. 1990; Harr et al. 1991), and TYPHOON–90. Typhoon Flo (9019) exhibited a marked deepening of −55 hPa/24 h (−80 hPa/48 h) during its "before-recurvature" stage in the western North Pacific to become a challenging target

* Bulletin of the American Meteorological Society, Vol.81, No.6, June 2000, 1341–1346.

for mesoscale numerical prediction. One important point is, hence, to examine how well current mesoscale models can simulate, and possibly predict, the explosive development of the tropical cyclone.

The intercomparison will focus firstly on the sensitivity of the track and the intensity of the simulated tropical cyclone (TC) to initial conditions, and secondly on sensitivity to horizontal resolutions. The evaluation is conducted against: 1) a set of best track data, 2) objective analyses enhanced with special observational data, 3) satellite-estimated precipitation, and 4) mesoscale fields analyzed based on aircraft observations.

This paper is organized as follows: The experimental design is explained in Section 2; In Section 3, evaluation methodology is introduced after examining quality of data for use in analysis and evaluation; Section 4 describes the synoptic setting and mesoscale fields; Section 5 presents results of evaluation and intercomparison. Some discussion is given in Section 6; Conclusions and remarks are provided in Section 7.

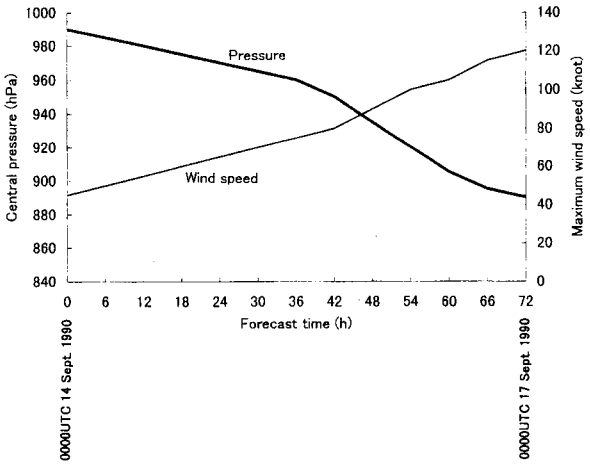

Fig. 1. Time series of Flo (9019)'s central pressure and maximum sustained wind speed (10-min average) according to the best track data by the RSMC Tokyo–Typhoon Center. T+00 h and T+72 h correspond to 0000 UTC 14 and 0000 UTC 17 September 1990, respectively.

2. Experimental design

The target event of explosive tropical cyclone development of −55 hPa/24 h commenced at 1200 UTC 15 September 1990. The initial time for simulation was set at 0000 UTC 14 September 1990 (see Fig. 1), 36 h prior to the commencement of the explosive development to examine if models can reproduce the explosive development with enough lead time. Prediction was made for 72 h from the initial time so that it covered the whole development stages. The time evolution of central pressure based on the Regional Specialized Meteorological Center (RSMC) Tokyo–Typhoon Center (JMA) Best Track data (Fig. 1) was characterized by two stages, the first half of the simulation window showing slow deepening, and the second half rapid deepening.

The 72-h simulation period was largely covered by some of the intensive observing periods (IOPs). Special observations included 6-hourly radiosondes, cloud drift winds by the University of Wisconsin, dropwindsondes, drifting buoys, and aircraft (NASA DC-8). Quality of each observational data is examined in Section 3.

Two sets of analyses were produced, one with JMA's Global Analysis system of T213/30 levels resolution (J-ANL) (JMA 1997) and the other with the National Centers for Environmental Prediction's (NCEP) Eta-Model Regional Analysis system of 48 km/38levels resolution (N-ANL) (Rogers et al. 1996). They were interpolated on to 0.5° × 0.5° latitude-longitude grid of 44 pressure levels mostly with 25 hPa intervals and the surface. These analyses were used as initial fields for all the participating models and as lateral-boundary conditions for regional models. The reason why we prepared two analyses for initial conditions was that we considered there was large uncertainty in the analysis fields to be used as initial conditions, because of the sparsity of observational data even during the special field experiments.

Furthermore, synthetic tropical cyclone vortices (tropical cyclone bogusing) introduced other uncertainties, which prompted us to make experiments to examine a state-of-the-art scheme of tropical cyclone bogusing. For this purpose we requested the GFDL/NOAA Hurricane Modeling Group to initialize tropical cyclones in the analyses with their sophisticated scheme (Kurihara et al. 1993; Bender et al. 1993b) by providing the tropical cyclone parameters in the Best Track data of the RSMC Tokyo–Typhoon Center, JMA. Thus a combination of two analyses with and without the GFDL bogusing produced four sets of initial fields. We note here that JMA's Global Assimilation employed its own simple, static TC bogusing scheme

(JMA 1997) in contrast with GFDL's dynamical bogusing scheme, which operated an axi-symmetric numerical model with appropriate forcing to obtain a quasi-balanced target vortex having a specified storm intensity and size. Both JMA's and GFDL's bogusings are capable of producing a balanced vortex which has a set of central pressure and wind radius (radius of 30 kt winds in this case) fairly close to a given set of these parameters, unless the analyzed central pressure is too low and/or the wind radius is too small for the storm structure to be resolved by the model grid, which is rarely the case. In this particular case for the study, since the radius of 30 kt winds of the target storm (225 nm = 417 km) was large enough compared to the model grid intervals, the storm size was well represented even in the coarser-mesh fields. Meanwhile, NCEP's Eta Model Regional Assimilation did not employ any TC bogusing. Thus, JMA's bogusing was activated in Exps. 1A50 and 1A20, GFDL's bogusing in Exps. 1B50, 1B20, 1D50, and 1D20, while no bogusing was used in 1C50 and 1C20 (Table 1). Differences between J–ANL and N–ANL and significant differences between JMA's and GFDL's bogus TCs will be described in Section 4. Participants were provided with these four initial fields including the two original analyses for the region shown in Fig. 2 or for the whole globe, depending on the configuration of the participating model.

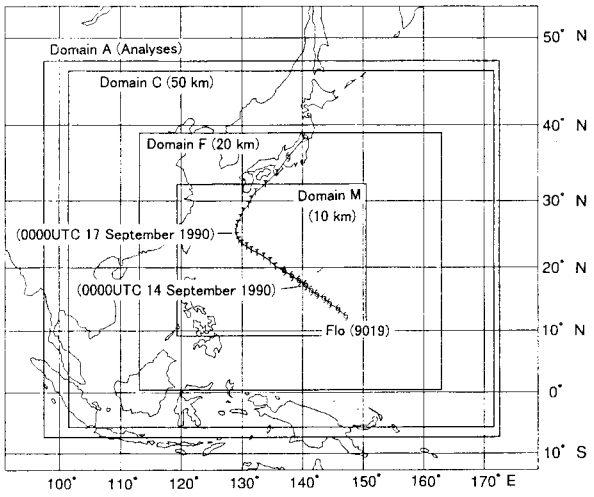

Fig. 2. Domain settings. Domain A for analyses distributed, Domain C for 50-km mesh runs, Domain F for 20-km mesh runs, and Domain M for 10-km mesh run.

The lateral boundary conditions were based on the same 6-hourly analyses as those used for the initial fields. We employed the strategy of Chouinard et al. (1994) to fix lateral boundaries in such a way that the outer simulation domain (see Fig. 2 for domain settings) was sufficiently large so that throughout the 72-hour simulation information at the lateral boundaries did not seriously affect the target system, which was located near the center of the domain. To calculate trajectories of the air parcels indicating contamination and released continuously along candidate lateral boundaries, we used a global tracer model including advection and diffusion processes (JMA 1997), which utilized JMA's analyses with 6-hour intervals for flow fields and diffusion coefficients calculated from the analysis variables for vertical mixing.

The outer, intermediate, and inner domains were covered with 50 km, 20 km, and 10 km resolution, respectively. A standard configuration of vertical levels was suggested to the participants. The 27 full-integer vertical levels in sigma coordinate were: .99625, .9875, .97625, .9625, .94625, .92875, .91125, .89375, .8725, .8425, .8000, .7500, .7000, .6500, .6000, .5500, .5000, .4500, .4000, .3500, .3000, .2500, .2000, .1500, .1000, .0500, .0125 from bottom to top. They were placed unevenly in such a way that higher resolutions were allotted to the planetary boundary layer (PBL). Domains for verification were a square of 40° (latitude) × 60° (longitude) (0°–40°N, 105°–165°E) with 0.5° resolution for synoptic scale, i.e., 50 km experiments, and a square of 20° (latitude) × 30° (longitude) (10°–30°N, 120°–150°E) with 0.25° resolution for meso scale, i.e., 20 km and 10 km experiments, both centered about the target TC in the horizontal and from the surface to 12.5 hPa with 24 pressure levels in the vertical. Participants provided prediction fields in these domains to the lead center, JMA.

In the first phase, the participants were requested to make nine experiments listed in Table 1. A combination of two analyses with two initializations (with and without the GFDL initialization) with two horizontal resolutions (50 km and 20 km) made eight experiments. They were designed to examine impacts of analyses, initializations, and horizontal resolutions. Experiment 2A20 was a 20 km experiment with the JMA analysis given for lateral boundary conditions instead of the prediction field of the corresponding coarse-mesh (50 km) run (Exp. 1A50). This experiment was designed to investigate the impact of specifying the lateral

Table 1. List of experiments.

phase		analysis for initial fields	TC bogus	horizontal resolution	vertical levels*	lateral boundary conditions
↑	(Exp. 1A50)	JMA Global	JMA	50km	27	analysis
	(Exp. 1B50)	JMA Global	GFDL	50km	27	analysis
	(Exp. 1C50)	NCEP Eta Regional	none	50km	27	analysis
	(Exp. 1D50)	NCEP Eta Regional	GFDL	50km	27	analysis
1st	(Exp. 1A20)	JMA Global	JMA	20km	27	Exp. 1A50 prediction
	(Exp. 1B20)	JMA Global	GFDL	20km	27	Exp. 1B50 prediction
	(Exp. 1C20)	NCEP Eta Regional	none	20km	27	Exp. 1C50 prediction
	(Exp. 1D20)	NCEP Eta Regional	GFDL	20km	27	Exp. 1D50 prediction
↓	(Exp. 2A20)	JMA Global	JMA	20km	27	analysis
2nd	(Exp. 1A10)	JMA Global	JMA	10km	27	Exp. 1A20 prediction

* A few models employ different number of vertical levels.

boundary conditions with analysis in comparison with nesting the 20 km model in the 50 km model prediction. The result showed that the impact of the different lateral boundary conditions was negligibly small in this particular case, owing to a good prediction of the synoptic field with the 50-km models, and hence no further mention will be made of it. In the second phase, the participants were requested to make one 10 km experiment (Exp. 1A10) from JMA's analysis, with nesting in the corresponding 20 km experiment (Exp. 1A20). Thus, the total of nine experiments, without including 2A20, were the standard ones, while some participants made additional experiments on their own.

The fourteen participating models are listed in Appendix A. The number of models participating in the 50 km resolution experiments ranged from 14 to 12, and that for 20 km resolution experiments from 12 to 10. Thus a majority of the models participated in the eight standard experiments consisting of a combination of the four initial fields with two horizontal resolutions, 50 km and 20 km. Eight models participated in Exp. 2A20. The number of models participating in the second-phase 10 km resolution experiment 1A10 was six. Besides these, some participating groups made additional experiments to examine impacts of horizontal/vertical resolutions, parameterizations of deep convection, non-hydrostatic effects, lateral boundary conditions, etc. This paper, however, focuses on the evaluation of the simulations within the standard experiments, resulting in the evaluation of 109 simulations in total. The additional experiments will be evaluated in further studies by individual participants.

3. Quality of data for analyses and evaluations, and evaluation methodology

In this section the quality of data for use in the analyses and evaluations is examined first, and then an evaluation methodology is briefly introduced.

3.1 Quality of data

The Global Analyses were produced at the Meteorological Research Institute (MRI), JMA with the Global Spectral Model combined with statistical interpolation method at 6-hour intervals of data insertion. The data available for the analyses were:

- on-line conventional data obtained through the Global Telecommunication System (GTS)

and

- off-line data, which included:
  - TOVS 1D-VAR data provided by European Centre for Medium-Range Weather Forecasts;
  - TCM-90/SPECTRUM/TYPHOON-90 data archived by the United States Office of Naval Research (ONR);
  - SATOB (cloud drift winds provided by the University of Wisconsin);
  - dropwindsondes;
  - drifting buoys;
  - aircraft (NASA DC-8); and,
  - intensive upper-air soundings.

Among the special field observational data, the drifting buoys had large biases while they had small standard deviations of differences from the first guess (Table A2), which allowed bias correction to make data useful for analysis. Cloud drift winds reprocessed by the University of Wisconsin, were a good source of data even though differences from the first guess were not very small: Root Mean

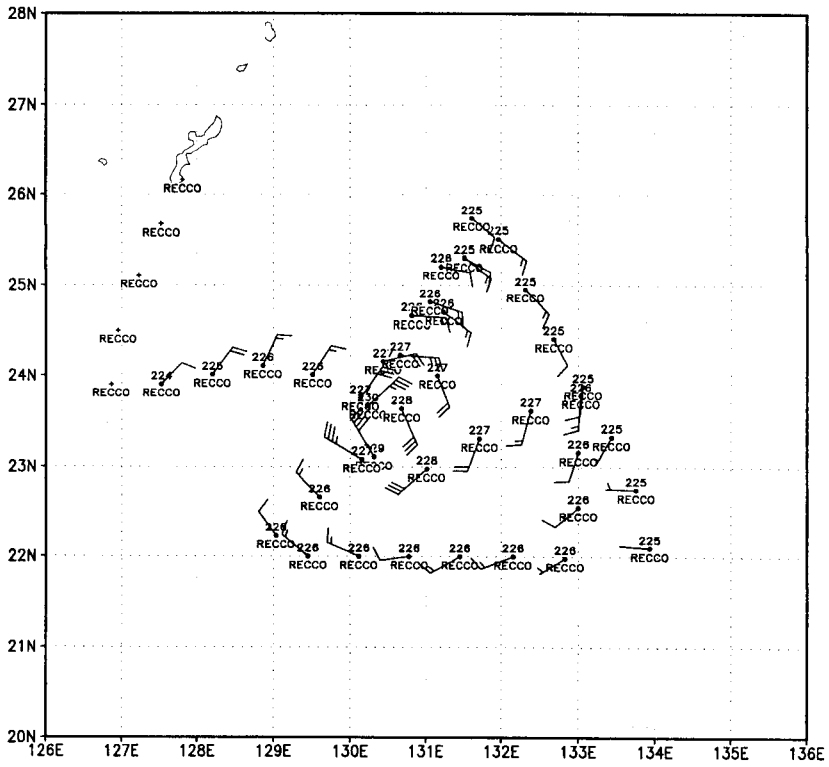

Fig. 3. NASA/DC-8 observations approximately at 200 hPa around 0600 UTC 16 September 1990. One wind barb is equivalent to $10\,m\,s^{-1}$ and unit of temperature is Kelvin.

Squares (RMSs) of differences from the first guess were approximately $5\,m\,s^{-1}$ and $8\,m\,s^{-1}$ at 850 hPa and 200 hPa, respectively. In middle- to upper-level geopotential, at five out of the seven intensive upper air (sonde) observing stations on the islands in the western North Pacific, were noted systematic positive deviations from the first guess (biases) (Table A3a) and relatively large biases and standard deviations of differences from the first guess were seen on the geopotential at the former USSR observation vessels (four columns from the left in Table A3b).

For analysis of mesoscale fields during IOPs, and evaluation of their predictions by the numerical models, exceptionally dense data taken by the NASA DC-8 aircraft were used (Fig. 3), although the flights were not very frequent and the flight level was basically single (approximately 200 hPa only). For making an objective analysis of temperature and wind at 200 hPa, a successive correction method was applied to the aircraft data of temperature and wind, with JMA's Global Analysis used as a first guess. We adopted this method instead of the statistical interpolation method used for making JMA's Global Analysis because the former can preserve more signals of mesoscale features than the latter which assumes the geostrophic balance as a constraint for analysis increments. The resultant objective analysis will be used for evaluation of numerical model predictions in Section 5 (see Fig. 15 later).

All the data mentioned above were used in making JMA's Global Analyses, while the same, but for TOVS 1D-VAR data, in making the NCEP Eta Model Regional Analyses. Dropsonde data, on the other hand, were regrettably not used for these objective analyses after careful consideration, because of huge differences from the first guess field. Note, however, here that sea-level pressure data estimated from dropsonde pressure measurements were used in the Best Track data analysis, which is used in the evaluation as shown below.

3.2 Evaluation methodology

There are three categories in the evaluation methodology. The first one is an evaluation of pa-

rameters characterizing TCs, i.e., center position, central pressure, maximum wind speed, radius of 30 kt wind, radius of 50 kt wind, against a posteriori analysis usually called Best Track data. We use the Best Track data produced by the RSMC Tokyo–Typhoon Center, JMA for this purpose. Generally speaking, storm center fixing hardly gives rise to much controversy, especially rarely for storms with an eye or a clear circulation center of spiral rain bands seen on a loop of satellite imagery. This is true in the case of Flo, where an eye formed at latest by 1800 UTC 15 September 1990, T+42 h into the simulation. In contrast, in the western North Pacific, where aircraft reconnaissance ceased in 1987, intensity parameters, i.e., central pressure and maximum sustained wind speed, may possibly have large errors, because they are mostly based on indirect estimates: measurements of satellite imagery features characterizing storm intensity combined with pattern recognitions (Dvorak 1975; 1984). Velden et al. (1998), who developed an objective tropical cyclone intensity estimation scheme, evaluated an operational scheme based on the standard Dvorak method with his new scheme against reconnaissance aircraft reports for homogeneous tropical cyclone cases in the North Atlantic in 1995 and 1996. He reported that the operational scheme has a bias of 5.9 hPa and a root-mean-square (RMS) error of 10.6 hPa in central pressure estimates. Since the intensity estimation scheme at JMA is almost identical to the operational scheme evaluated by Velden, we take into account errors of these magnitudes when using intensity data from the Best Track in the evaluation of tropical cyclone intensity simulations. For wind radii analysis, satellite cloud track winds delivered once a day are a major data source, besides Ship, Synop, and Buoy reports of surface winds. These data normally show fair coverage for the analysis of radius of 30-kt (approximately 15.4 $m\,s^{-1}$) winds, while they do relatively poor coverage for 50-kt (approximately 25.7 $m\,s^{-1}$) winds, which exist closer to the tropical cyclone center, where low-level cloud tracking often fails due to dense cover of high clouds and reports of direct measurements are relatively rare. To circumvent the data sparsity problem for the analysis of radius of 50-kt winds, JMA employs the statistical relationship between tropical cyclone central pressures and radii of 50-kt winds. The relationship is represented by three curves, each representing large, medium, and small storms. Therefore, accuracy of 50-kt wind radii, which are mostly based on the statistical relationship with intensity, is not as good as that of 30-kt wind radii, which are mostly based on direct observations and/or indirect measurements of wind (cloud tracking).

The second evaluation category is synoptic-scale conventional verification statistics against the objective analyses. In these kinds of tropical cases, we calculate absolute wind correlations between the simulation and observation at lower and upper troposphere as representing accuracy of predictions of synoptic fields.

The third category concerns mesoscale prediction fields. It is two-fold: statistical verification of precipitation with equitable threat scores (Schaefer 1990; Gandin and Murphy 1992; Mesinger and Black 1992; Rogers et al. 1996); and mesoscale evaluation against an objective analysis specially made at 200 hPa on the basis of the NASA DC-8 aircraft observations.

4. Synoptic setting and mesoscale fields

The synoptic setting at 0000 UTC 14 September 1990, the initial time of the simulation, is shown with the two sets of analysis fields; one by the Japan Meteorological Agency (JMA), and the other by the National Centers for Environmental Prediction (NCEP) (Fig. 4). In the low to mid levels, the large-scale monsoonal trough existed, which bred two tropical cyclones Ed (9018) and Flo (9019) successively. It was flanked by an east-west oriented subtropical ridge on its north side. The ridge persisted until 0600 UTC 16 September 1990, after which it was split by Flo's northward intrusion. In the upper troposphere (200 hPa), some anticyclonic and cyclonic circulations were noted: One anticyclonic circulation represented the eastern portion of the quasi-stationary Tibetan High centered around (27°N, 110°E). Another just east of Flo centered around (16°N, 141°E) was moving slowly to the west, expanding its area. A large-scale upper-tropospheric low (cyclone) centered at (26°N, 157°E), at 1800 UTC 14 September 1990 migrated slowly west-southwestward, holding a distance of approximately 20 degrees in longitude with Flo (figures not shown). Meanwhile, a smaller-scale upper-level cyclone centered around (25°N, 139°E) at 0000 UTC 14 September 1990 also migrated slowly west-southwestward. Flo's explosive deepening occurred just east-northeast of this smaller-scale cyclone, a tropical upper-tropospheric trough (TUTT) cell, which might have helped expansion

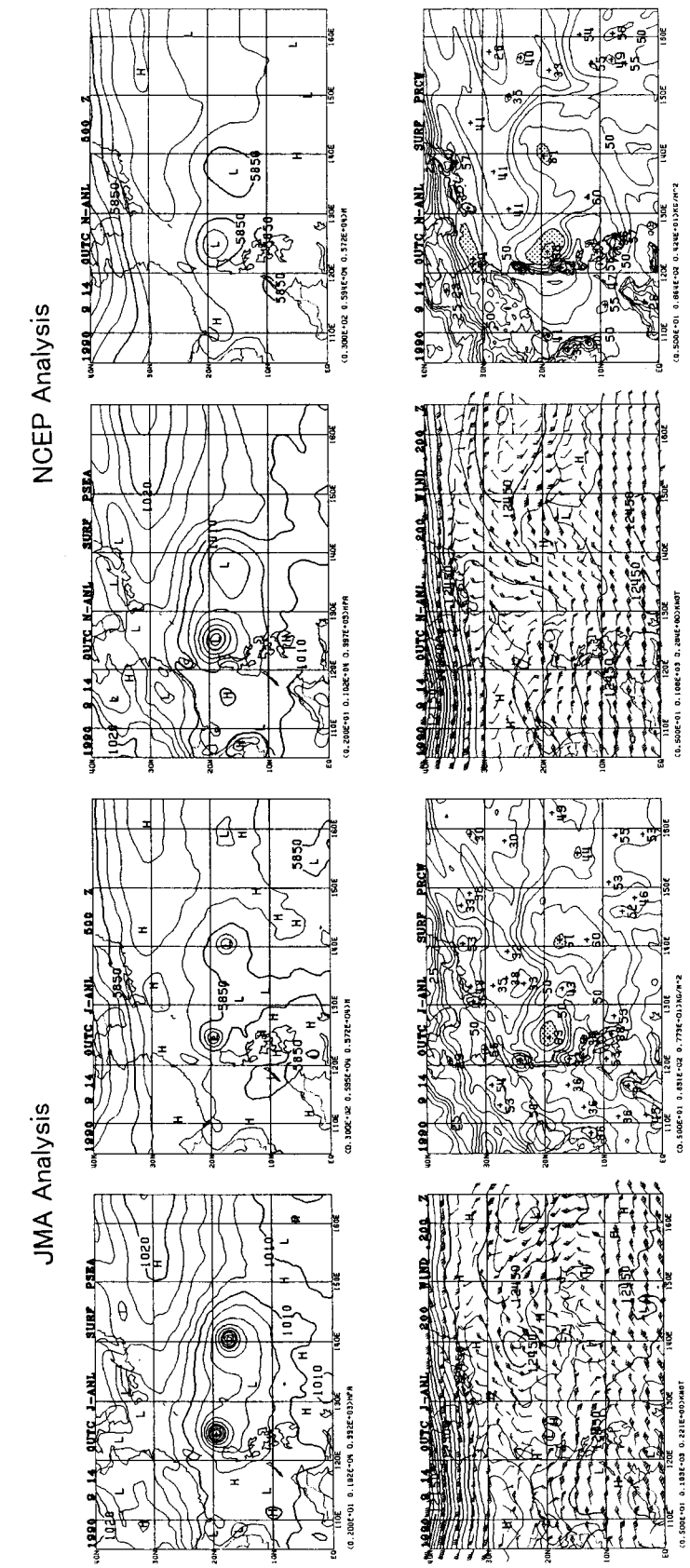

Fig. 4. JMA's Global Analysis (J–ANL, left two columns) and NCEP's Eta Regional Analysis (N–ANL, right two columns) at 0000 UTC 14 September 1990. Sea-level pressure (hPa) (upper left), 500 hPa height (gpm) (upper right), 200 hPa height (gpm) with winds (lower left), and precipitable water (mm) (lower right) are shown.

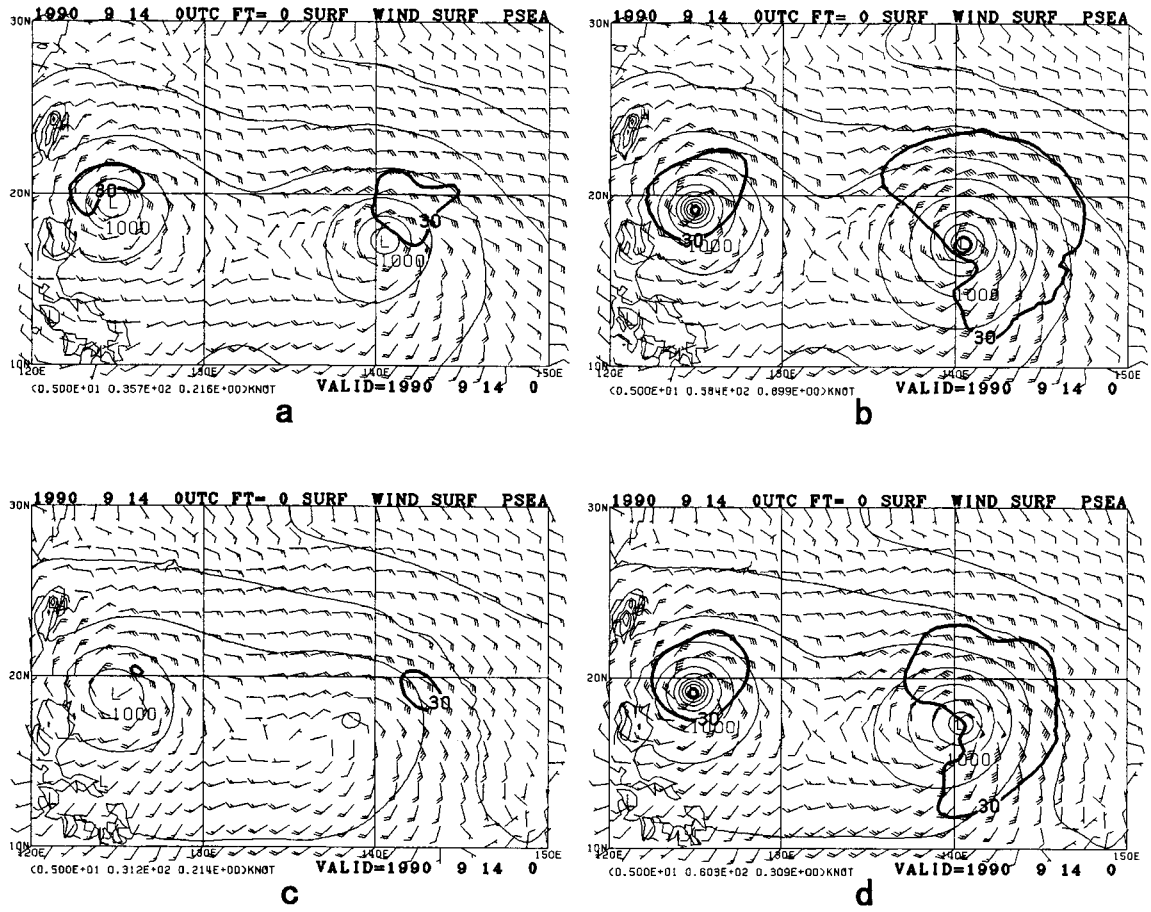

Fig. 5. Sea level pressure (thin sold lines) and surface winds in the four initial fields. Contour intervals for pressure are 4 hPa, wind notation is conventional. Isotachs of 30 kt are drawn with thick solid lines. (a) JMA analysis with JMA bogusing (for Exp. 1A), (b) JMA analysis with GFDL bogusing (for Exp. 1B), (c) NCEP analysis without bogusing (for Exp. 1C), (d) NCEP analysis with GFDL bogusing (for Exp. 1D). Flo (9019) and Ed (9018) are seen on the right and the left, respectively, in each panel.

of the western part of the anticyclone. At around 1200 UTC 16 September, Flo started recurving to the northwest and then to the north by 0600 UTC 17 September under the influence of the splitting of the subtropical ridge (figures not shown). Thus the substantial portion of the explosive development occurred before recurvature of the storm.

By comparing the two analyses at 0000 UTC 14 September, we have found some significant differences between them. Recall here that TC bogusing is activated for the two tropical cyclones Ed and Flo in JMA Analysis, while it is not in NCEP Analysis. Positive differences (NCEP–JMA) in sea-level pressure and 500 hPa height fields with anti-cyclonic circulation differences (NCEP–JMA) (figures not shown) exist in a rectangle area (12–22°N, 144–152°E) near east of Flo. In association with these anticyclonic circulation differences, we have negative precipitable water differences (NCEP–JMA) in the same rectangle area. These may produce significant differences in precipitation, especially in the outer region of Flo. Another notable difference is that the smaller-scale upper-level cyclone centered around (25°N, 139°E) is less defined in NCEP Analysis than in JMA Analysis, which may influence Flo's temporal evolution in intensity. The other difference is that NCEP Analysis fields are generally smoother than JMA Analysis fields, even though analysis grid of NCEP's Eta-Model Regional Analysis system (48 km) is slightly finer than

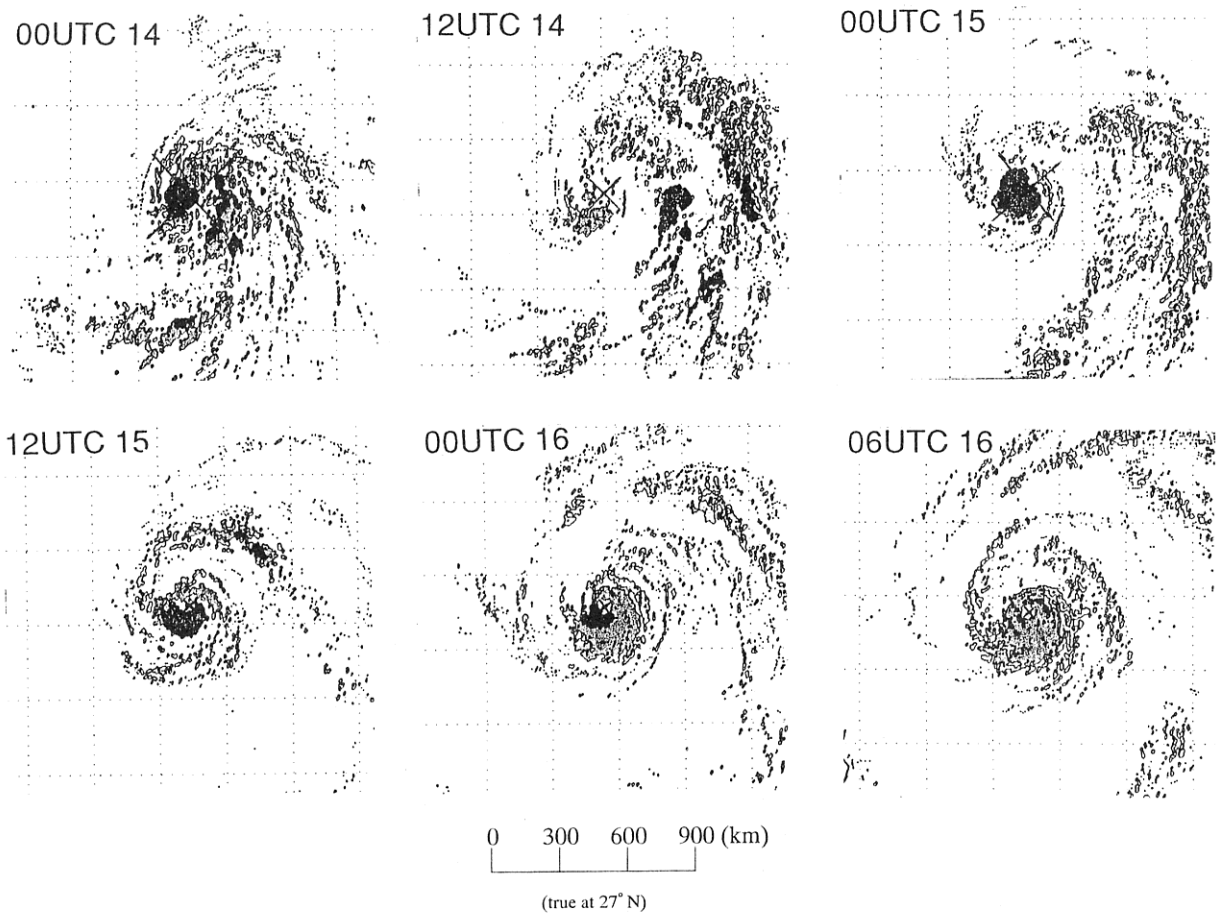

Fig. 6. Distribution of GMS–IV–estimated convective precipitation in 15 × 16.7 deg window centered at typhoon center at 0000 UTC 14, 1200 UTC 14, 0000 UTC 15, 1200 UTC 15, 0000 UTC 16, and 0600 UTC 16 September 1990 (data provided by Toshiyuki Kurino).

that of JMA's Global Analysis system (~55 km).

We also compare initial fields between the two bogusing schemes, JMA's and GFDL's. Figure 5 shows sea-level pressure and surface winds in the four initial fields. It is readily noticed that the TC circulation in the initial field for Exps. 1As (1A50, 1A20, 1A10) is weaker than those for Exps. 1Bs (1B50, 1B20) and 1Ds (1D50, 1D20). A major reason why there is a difference in the TC circulation at the initial time between the two boguses is that gradient wind speed (at the surface), instead of surface wind speed, is set at 30 kt at the analyzed "radius of 30 kt winds" in JMA's bogus, while surface wind speed (at 10 m height) itself is set to 30 kt at the analyzed "radius of 30 kt winds" in GFDL's bogus. As a result, surface winds at the analyzed "radius of 30 kt winds" are systematically weaker than 30 kt in JMA's bogus, as is usually the case, while those are almost equal to 30 kt in GFDL's bogus, at the initial time.

To elucidate features of the precipitation field associated with Flo, precipitation was estimated by Toshiyuki Kurino at the Meteorological Satellite Center (MSC), JMA with the Adler and Negri (1988) scheme using the Geostationary Meteorological Satellite (GMS–IV) infrared data. The scheme produced estimates of not only convective, but also stratiform precipitations. However, stratiform portions were quantified only in two values, i.e., 0 mm h^{-1} and 2 mm h^{-1} due to limitations inherent to infrared data and they carry almost no quantitative information unlike convective portions which ranged continuously from 0 mm h^{-1} to more than 20 mm h^{-1}. We decided to use only the con-

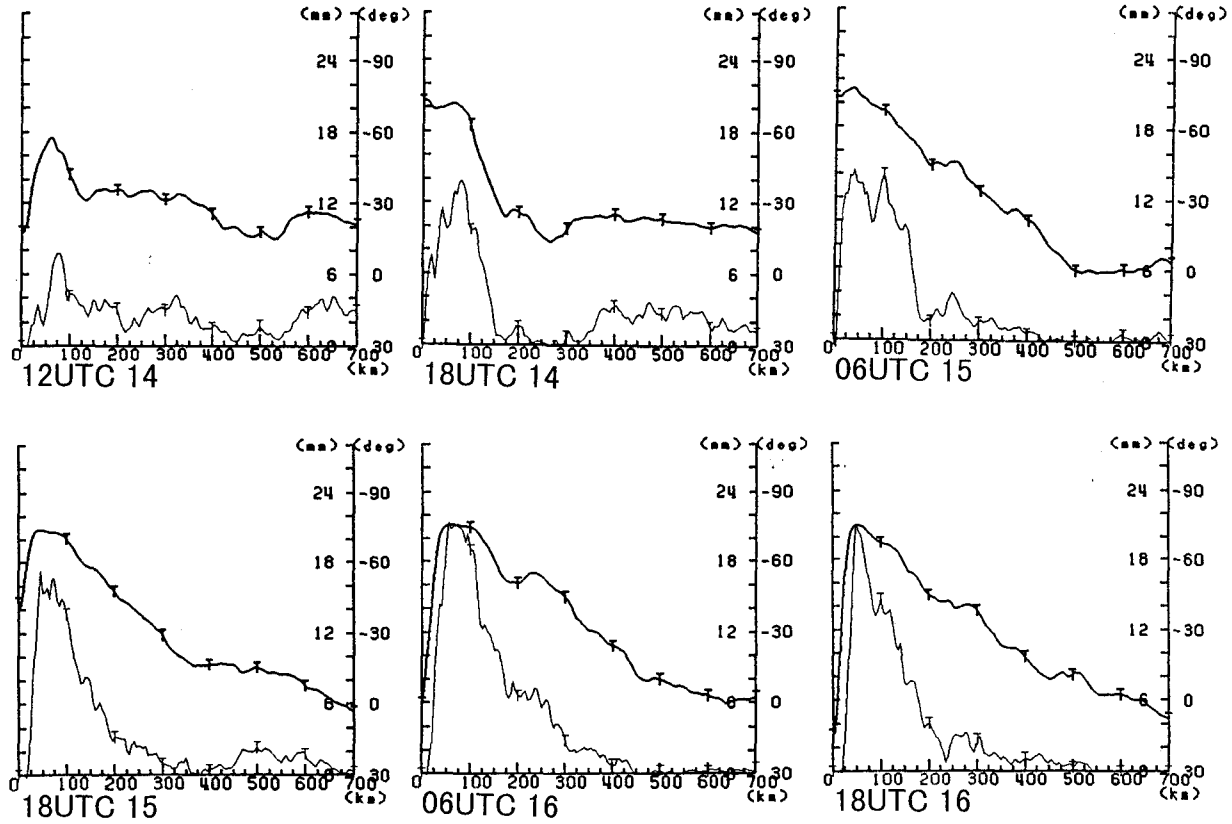

Fig. 7. Radial distributions of equivalent black body temperature (T_{BB}) (thick solid line, unit: deg) and satellite-estimated 1-hour convective precipitation (thin solid line, unit: mm) at 1200 UTC 14, 1800 UTC 14, 0600 UTC 15, 1800 UTC 15, 0600 UTC 16, and 1800 UTC 16 September 1990. Note that T_{BB} is plotted invertedly.

vective portions of the precipitation estimates for evaluation of the model simulations, considering the difference in availability of quantitative information.

Several mesoscale features are noted in a time series of the satellite-estimated convective precipitation (Fig. 6). The first 24 h period was characterized by highly asymmetric nature of scattered convective precipitation, i.e., much more precipitation scattered on the east side of Flo's center than on the west side. Another notable feature was successive propagation of outer broad bands of convective precipitation. During the development stage, the first outer broad band of convective precipitation was organized at 1200 UTC 14 September 1990, about 300 km east-southeast of the typhoon center, propagated eastward and also northeastward afterwards, and dissipated around 1200 UTC 15 September. The second one was organized at 1200 UTC 15 September about 400 km northeast of the typhoon center. It propagated northeastward, and dissipated around 1200 UTC 16 September far northeast of the typhoon center (figure not shown). Its western portion with west-southwest to east-northeast orientation survived longer than the eastern portion, along the southern coasts of the Japanese islands, presumably owing to the deformation field along the baroclinic zone associated with the mid-latitude westerlies. Meanwhile, near the typhoon center, convective precipitation became concentrated to form a precipitation core around 1800 UTC 14 September. A maximum in equivalent black body temperature (T_{BB}) (Fig. 7) first appeared at the center, indicating the formation of an eye of the typhoon, around 1800 UTC 15 September (T+42 h), when the analyzed central pressure fell to 950 hPa. The small eye persisted for the rest of the simulation period.

Table 2. Experiments performed by the models for Exps. 1A50, 1A20, 1A10, 1B20, 1C20, and 1D20 in a matrix form. The matrix is filled with central pressure changes of Flo in individual models for each of the two stages (slow deepening stage from T+12 h to T+36 h and rapid deepening stage from T+42 h to T+66 h), along with central pressure values near the end of the second stage (T+66 h).

Exp. / Model	1A50		1A20		1A10		1B20		1C20		1D20	
	Pc change 12-36h/42-66h	Pc 66h	Pc change 12-36h/42-66h	Pc 66h	Pc change 12-36h/42-66h	Pc 66h	Pc change 12-36h/42-66h	Pc 66h	Pc change 12-36h/42-66h	Pc 66h	Pc change 12-36h/42-66h	Pc 66h
(Best Track)	-20 / -55	895	-20 / -55	895	-20 / -55	895	-20 / -55	895	-20 / -55	895	-20 / -55	895
TYM	-5 / -17	969	-16 / -26	943	-16 / -21	946	-9 / -10	954	-2 / +1	1002	-7 / -5	974
Unified Model	-6 / -6	979	-10 / -2	975	-22 / -17	948	-20 / -1	956	-2 / -1	1001	-11 / -3	967
BOLAM	-7 / -23	960	-25 / -38	917	-26 / -55	890	NO		NO		-9 / -16	953
RSM/NCEP	-5 / 0	989	-5 / -3	983	NO		-5 / -4	966	-3 / 0	1001	-5 / +1	983
EM10M	-3 / -5	984	-11 / -31	942	NO		-48 / +3	926	*		-68 / -21	856
MC2	-5 / -5	983	-9 / -3	978	-11 / -8	965	-20 / -10	940	-4 / -1	998	-17 / -13	947
GEM	-8 / -8	975	-13 / -5	969	-16 / -1	967	-21 / +1	947	-7 / -2	992	-25 / -6	945
HIRLAM	-1 / +1	991	-3 / +1	987	NO		-1 / +4	977	-2 / +1	1000	+1 / 0	982
Eta	-1 / -1	992	-2 / -1	988	NO		-2 / -2	972	-1 / -1	1001	-1 / 0	984
DARLAM	-7 / -4	988	-17 / -4	967	NO		-10 / -5	952	-6 / +1	999	-8 / -5	964
CSIRO-S	-2 / 0	995	-5 / -5	984	NO		-1 / +1	976	NO		NO	
JSM	-4 / -9	982	-17 / -18	948	-11 / -20	950	-14 / -18	937	-2 / -4	996	-9 / -9	968
COAMPS	-2 / -5	983	NO		NO		NO		NO		NO	
RSM/NCMRWF	0 / +1	998	NO		NO		NO		NO		NO	
number of models	14		12		6		11		10		11	

* TC center tracker failed

5. Evaluation and intercomparison of simulations

In this section, evaluation of the simulations and intercomparison of the models are described, including an examination of heating and moistening profiles by moist physical processes.

Table 2 summarizes experiments performed by the models for Exps. 1A50, 1A20, 1A10, 1B20, 1C20, and 1D20 in a matrix form, including some information on TC intensity prediction performance. All of the fourteen models participated in the four 50 km experiments except for CSIRO–S in Exps. 1C50 and 1D50, and NCMRWF's RSM in Exps. 1B50, 1C50, and 1D50.

5.1 Tropical cyclone parameters and wind distribution

First of all, several parameters characterizing the tropical cyclone are verified against the RSMC Tokyo–Typhoon Center's Best Track data. The parameters verified include center position (track), central pressure, radius of 30 kt winds and radius of 50 kt winds. In Fig. 8, Flo's predicted tracks in the 20-km resolution experiments are shown. The corresponding Best Track is denoted by a dashed line with tropical cyclone marks in each panel. Those in the 50-km resolution experiments are not shown because differences in track between the two horizontal resolutions (e.g., Exp. 1A50 vs. Exp. 1A20) are negligibly small. The models succeed in simulating the typhoon's northwestward translation with biases, more or less, in all of the eight standard experiments. It is of interest to note that in each experiment most of the models produce very similar tracks to each other, while differences in tracks are relatively large among the four initial conditions. In this particular case, where the typhoon was mostly in the stage before recurvature, the impact of initial conditions on track is much larger than that of horizontal resolutions, and almost no significant differences in track are observed among the models in each experiment. In a comparison among the initial conditions, we find that the mean positional errors (figures not shown) at T+72 h are smallest in Exp. 1A, largest in Exps. 1C and 1D, and in between in Exp. 1B.

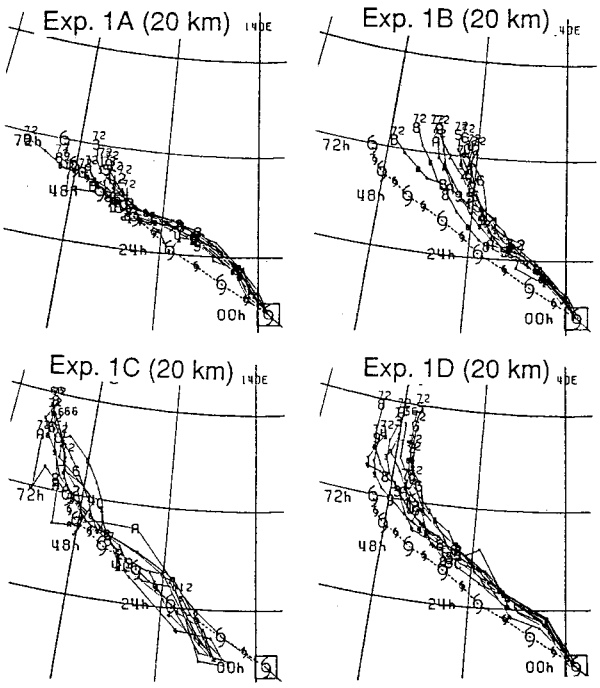

Fig. 8. Track predictions by models (solid lines) in the four 20 km-resolution experiments against the Best Track (thick dashed with TC marks) provided by RSMC Tokyo–Typhoon Center.

Tracks predicted in Exps. 1B and 1D, which were initialized with the GFDL bogusing, have rightward biases when looking in the direction of translation (east-northeastward biases in Exp. 1B and north-northeastward biases in Exp. 1D), while those in Exp. 1C have mostly large northward biases and those in Exp. 1A mostly east-southeastward biases. The northward (or north-northeastward) biases in Exps. 1C and 1D, which used NCEP Analysis as their initial fields, may be associated with the anticyclonic circulation anomaly in NCEP Analysis in comparison with JMA Analysis, which was mentioned in Section 4. Actually we find southerly flow anomalies (NCEP–JMA) around Flo's center on the western portion of the anticyclonic circulation anomaly at a middle level (figure not shown).

Next we verify evolutions of Flo's central pressure with the corresponding Best Track data (Fig. 9 and Table 2). Here we examine results of the 20-km experiments. The impact of horizontal resolution will be described at the end of this subsection. We find several notable aspects in the intercomparison of the intensity predictions. First, most of the models predict developments of the tropical cyclone in Exps. 1A20, 1B20 and 1D20 even though their degrees are various among the models, while no development is seen in any models in Exp. 1C20. This suggests that a TC bogusing is crucial for the prediction of a tropical cyclone in its early developing stage in a data-sparse area. Second, we note an obvious tendency for almost all the models to underpredict the intensity of the tropical cyclone more or less. One of the major reasons for this underprediction of intensity must be that the horizontal resolution is insufficient to resolve and simulate inner-core structures of a very intense tropical cyclone whose horizontal scale ranges down to a few tens of kilometers as that for eyewall clouds. The only exception in intensity prediction is DWD's EM10M, in which the central pressure of the typhoon attains near 920 hPa in Exp. 1B20, and below 860 hPa in Exp. 1D20. These, apparently realistic, very low central pressures reproduced in DWD's EM10M, however, should be carefully examined further in the future since the model is an obvious "outlier" among the models in central pressure prediction. In Exp. 1A20, in contrast, EM10M is not an outlier, showing a fairly good evolution of central pressure.

Third, the other important point is that the qualitative feature of the time evolution of central pressure, i.e., slow deepening in the first half and rapid deepening in the second half, is reproduced best by some models in Exp. 1A20 among the four 20 km experiments, even though the deepening is still much underpredicted. The reproducibility of central pressure evolution can be evaluated to the first-order approximation by verifying central pressure changes for each of the two stages against those of the Best Track data in Table 2. The matrix of Table 2 carries central pressure changes of Flo in individual models for each of the two stages (the slow deepening stage from T+12 h to T+36 h and the rapid deepening stage from T+42 h to T+66 h) mentioned in Section 2, along with central pressure values themselves near the end of the second stage (T+66 h). The table shows good predictions of pressure change in the first stage (slow deepening), but poor predictions in the second stage (rapid deepening) common in many of the models in Exps. 1B20 and 1D20. Central pressures in most of the models fall around the Best Track curve in the first half of the simulation but nearly level

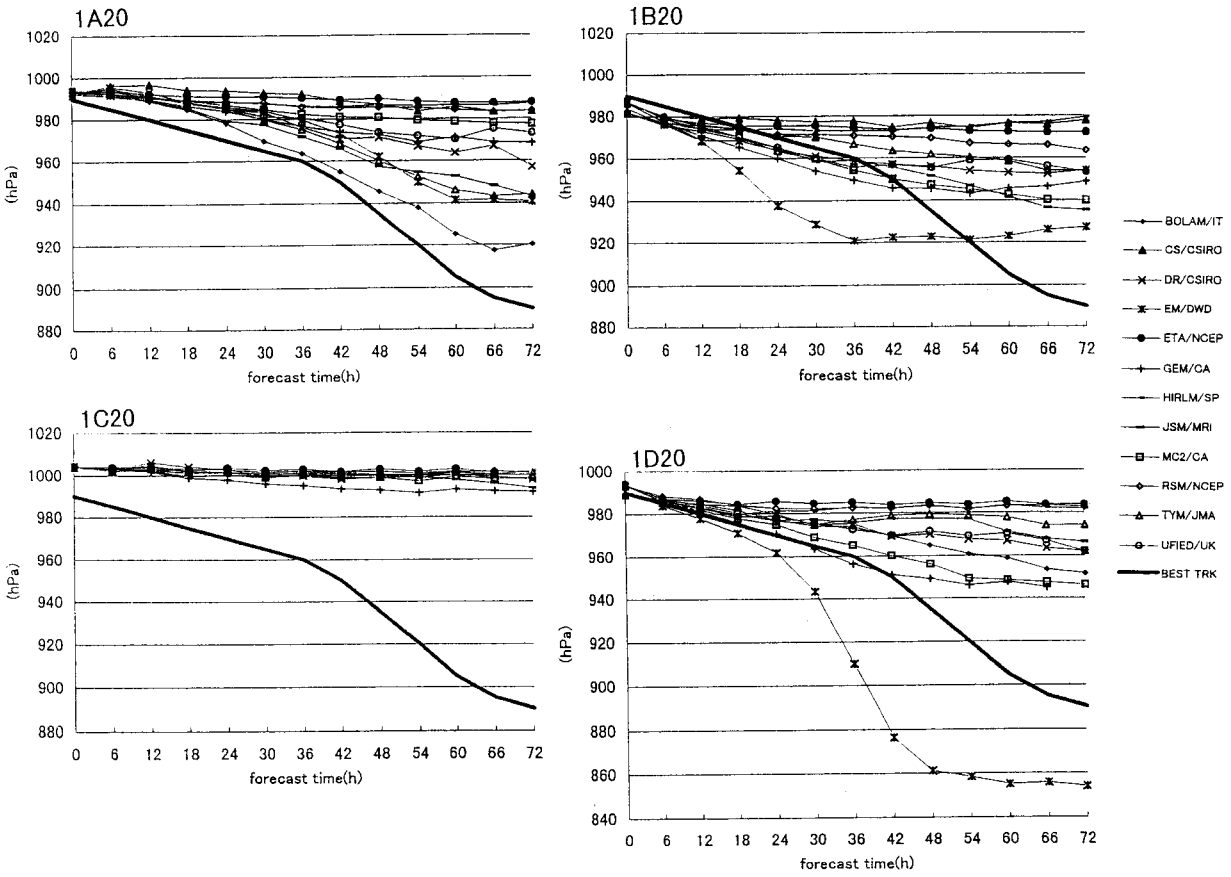

Fig. 9. Time series of intensity (central pressure) predictions by models (thin solid lines) in the four 20 km-resolution experiments against the Best Track data (thick solid line).

off afterward, failing to enter the rapid deepening stage. Meanwhile, fairly good predictions of pressure change are seen both in the two stages in some of the models, including ISAO–CNR's BOLAM, apparently the best performer in this particular case, in Exps. 1A20 and 1A10.

To verify wind profiles, see Fig. 10, which compares profiles of wind speed at the surface at T+54 h (valid at 0600 UTC 16 September 1990) in each 20-km experiment with some Best Track parameters for winds; maximum 10-minute average wind speed, radius of 50 kt winds, and radius of 30 kt winds. The time for validation (T+54 h) is chosen as it is representative of the second stage (rapid deepening) of central pressure evolution. When averaged among the models, the typhoons in Exps. 1B20 and 1D20 have larger scales than those in Exp. 1A20, where radii of maximum wind speed fall below 100 km in some models. The smaller radii of maximum wind speed in Exp. 1A20 are more consistent with the observation of a small eye of Flo with its radius of a few tens of kilometers (see Fig. 6). Thus the structure in the inner core region of the typhoon is better simulated in Exp. 1A20 than in Exps. 1B20 and 1D20 and almost not in Exp. 1C20. On the other hand, radius of 50 kt winds and radius of 30 kt winds are both simulated better in Exps. 1B20 and 1D20 than in Exp. 1A20, in which both radii are underestimated. This feature of the typhoon in Exp. 1A20 may be explained at least partly by the fact that the circulation at the initial time in Exp. 1A20 is weaker than those in Exps. 1B20 and 1D20 (Fig. 5). Storm structure in the outer region around the analyzed "radius of 30 kt winds" can certainly influence prediction of storm track, and probably intensity as well. The systematic difference in wind field between Exp. 1A20 and Exp. 1B20 (or Exp. 1D20) is

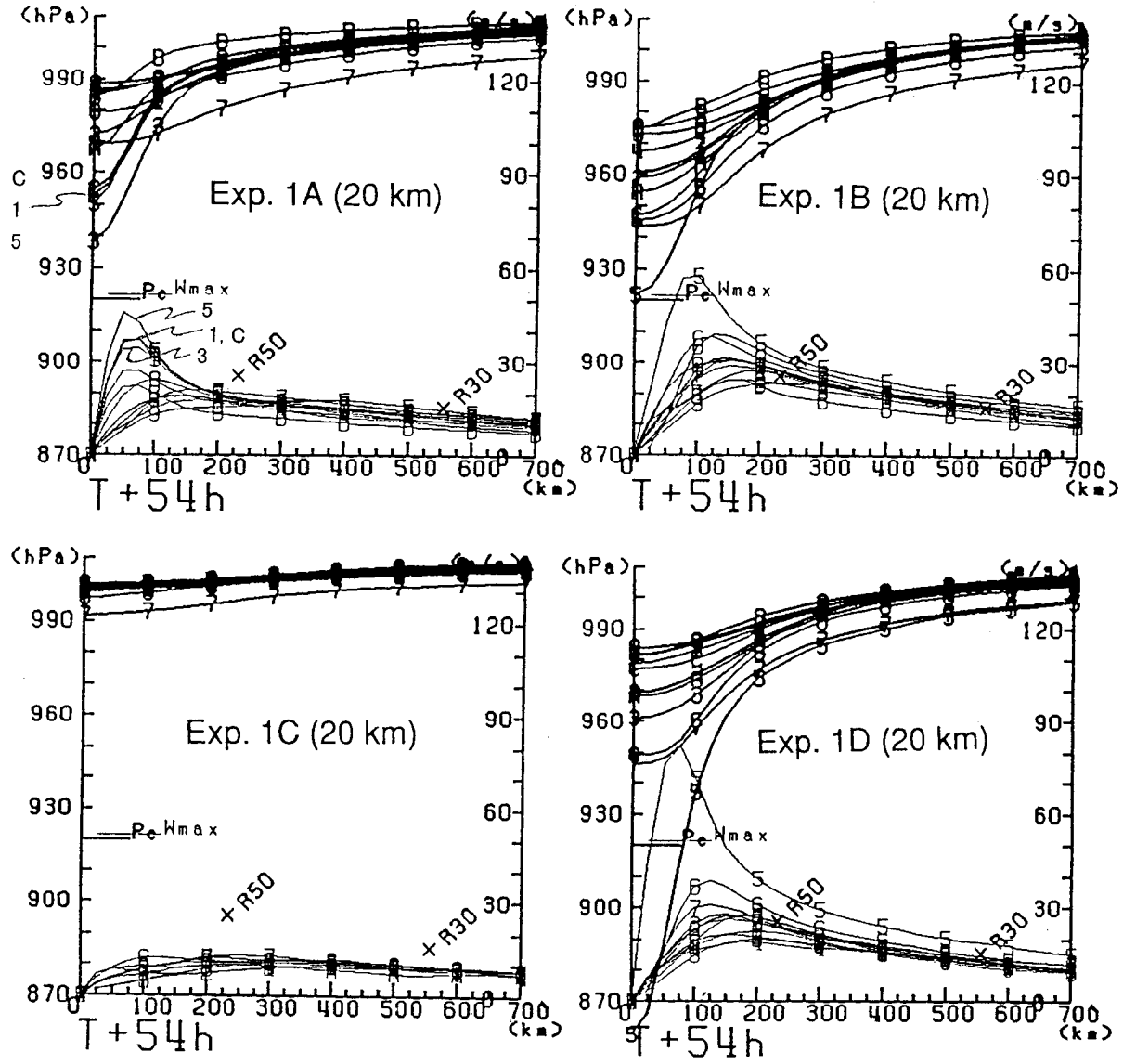

Fig. 10. Radial profiles of axi-symmetric components of sea-level pressure (thick lines, unit: hPa) and surface wind speed (thin lines, unit: $\mathrm{m\,s^{-1}}$) in the four 20 km-resolution experiments against the Best Track data, among which central pressure (P_c), maximum sustained wind speed ($W_{\max}$, 10-min. average), radius of 50 kt winds (R_{50}), and radius of 30 kt winds (R_{30}) are plotted.

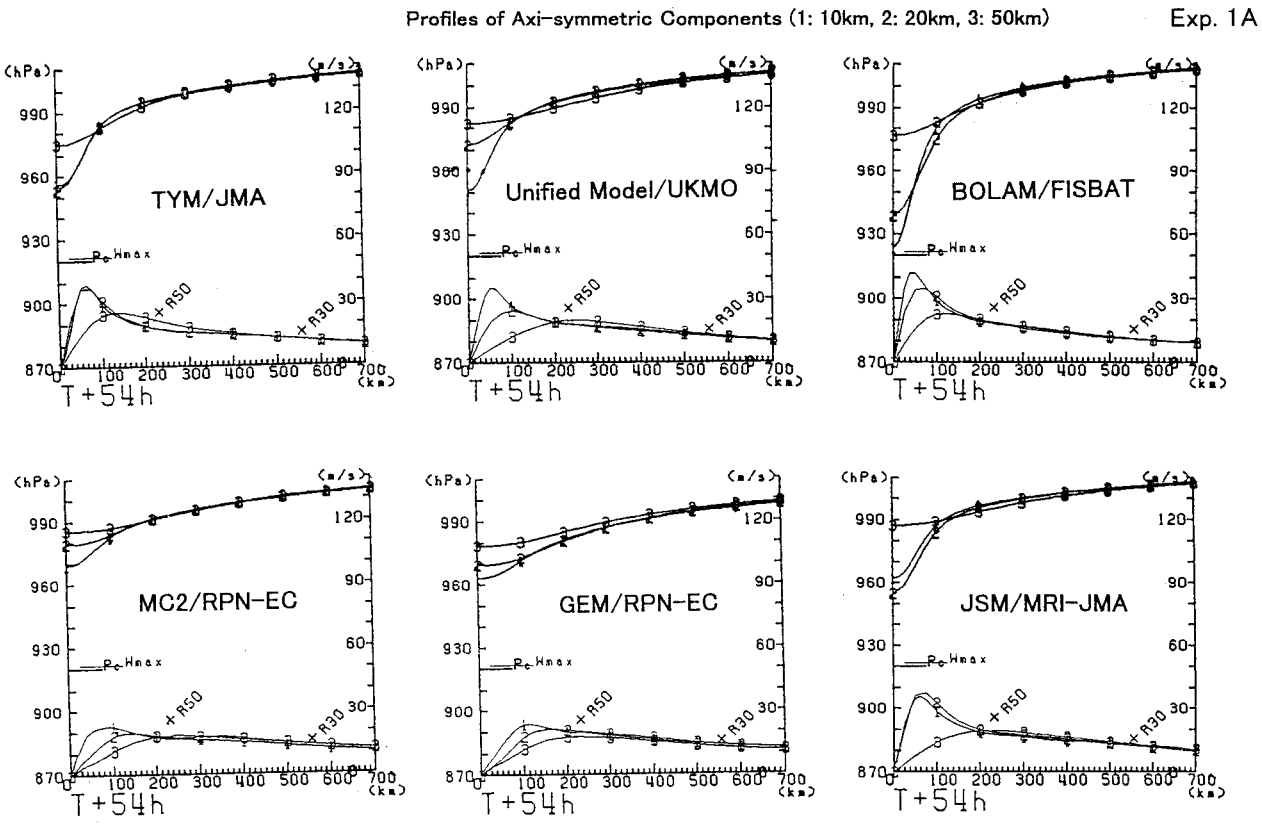

Fig. 11. Same as Fig. 10, but for 10-km (1), 20-km (2), and 50-km (3) experiments in Exp. 1A with six models.

also apparently related to a systematic difference in precipitation distribution, as shown later in this section.

At the end of this subsection, we examine the impact of the horizontal resolution on Flo's intensity prediction. The same kind of surface wind speed and sea-level pressure profiles as Fig. 10 are prepared for comparison of the simulations in Exp. 1A among the three horizontal resolutions for six models participating; JMA's TYM, UKMO's Unified Model, ISAO-CNR's BOLAM, RPN's MC2, RPN's GEM, and MRI's JSM (Fig. 11). The profiles show that as the horizontal resolution is changed from 50 km through 20 km to 10 km, maximum wind speeds increase, radii of maximum winds decrease, and central pressures decrease more or less, while magnitudes of the changes vary among the models. Thus, in Exp. 1A, the impact of horizontal resolution on tropical cyclone intensity is clearly discernible in the spatial range between 50 km and 10 km. Note here that the pair of brother models at JMA, JMA's TYM and MRI's JSM show little differences between Exps. 1A20 and 1A10, unlike the other models.

5.2 *Synoptic-scale evaluation*

Predictions of synoptic-scale fields in 50 km simulations are evaluated by calculating absolute correlation coefficients of winds at 200 hPa and 850 hPa against the two analyses J-ANL and N-ANL (figures not shown). Correlation coefficients are generally high, mostly above 0.8 even at the end of the simulations (T+72 h). An interesting feature which we have found is that those against N-ANL are larger than those against J-ANL, except for the early prediction hours. This is true even in Exps. 1A and 1B in which J-ANL is used as the initial conditions. This may probably be explained by the fact that, as mentioned in Section 4, J-ANL includes more signals of smaller-scale features (than N-ANL), which are harder to predict than large-scale components. Thus, a caution is

needed in using absolute correlation coefficients of winds against analyses in evaluation of predictions in the synoptic scale.

It is interesting to note here to what extent the accuracy of synoptic-scale prediction is correlated with accuracy of typhoon intensity prediction. To explore this, we have examined correlation between time-mean correlation coefficients of central pressure with the Best Track data versus time-mean correlation coefficients of 6-hourly 200-hPa wind predictions in the four 20 km experiments against the JMA Analysis. We do not see any significant correlation between the prediction performance of Flo's central pressure change and that of the synoptic field. This result suggests that accurate prediction of wind fields for a synoptic scale only is not necessarily sufficient for accurate prediction of tropical cyclone intensity.

5.3 Mesoscale evaluation

First we examine total precipitation simulated in each model by evaluating them with the satellite-estimated convective precipitation introduced in Section 4. We do not deal with simulated precipitation separately in convective type and in stratiform type, partly because we have observed that partition into the two categories varies so much from model to model, depending mainly on moist physical processes employed, especially cumulus parameterization, as shown later in this section, and partly because no quantitative stratiform precipitation estimates are available.

Distributions and amounts of precipitation show a wide variety depending on models and initial conditions (Fig. 12). A complex combination of model physics, including cumulus parameterization and planetary boundary layer schemes among the assimilation models, the initialization model, and the prediction models, should be involved in this variety. One significant difference is marked between the pair of Exps. 1A20 and 1B20 and the pair of Exps. 1C20 and 1D20 (Fig. 12b). Precipitation in the latter pair is much less east of the 140°E longitudinal line than in the former pair. This difference in precipitation can be attributed to the difference in precipitable water field at the initial time (see Fig. 4), which has been pointed out in the comparison of the two analyses in Section 4. A majority of the models in all the experiments, nonetheless, succeed more or less in simulating the major outer rain band with northwest-southeast orientation to the east-northeast of the typhoon center besides the precipitation core near the center. This may be related to the fact that synoptic-scale fields are in general fairly well reproduced in each model.

To evaluate the predictions of precipitation, we calculate equitable threat scores (ETSs) (see Appendix C for the definition of ETS) for the 20 km simulations (Fig. 13) against the satellite estimated precipitation introduced in Section 4. The ETSs are calculated with a threshold of 10 mm $(6\,\mathrm{h})^{-1}$ separately in the inner-core region ($r < 200$ km), and in the outer region (200 km $\leq r <$ 700 km), where r is the distance from the typhoon center. Note here that not only representations of axi-symmetric components, but also those of asymmetric components, are evaluated with the scores. The figure shows that modest skills are found in both regions only in several models in Exp. 1A20. In the other experiments (Exps. 1B20, 1C20, and 1D20) little skill is found in the inner-core region while modest skill exists in the outer region, except for Exps. 1B20 and 1D20 with DWD's EM10M. The better scores for the inner-core region in Exp. 1A20 than in the other experiments is consistent with the fact that the typhoon intensity change is better predicted in Exp. 1A20 than in the other experiments in terms of time series of central pressure. DWD's EM10M, which is an obvious outlier in the intensity prediction in Exps. 1B20 and 1D20 (Fig. 9), shows relatively high skills in the inner-core region in these experiments unlike the other models. EM10M is the only model of all the participating models that succeeds in simulating concentration of precipitation in the inner-core region in these experiments. However, it overpredicts precipitation amounts so much that the central pressure becomes too low for the early and middle prediction hours in Exp. 1B20 and for the entire prediction hours in Exp. 1D20. Such overdevelopments in EM10M have seriously affected mesoscale prediction fields even at an upper level (200 hPa), which can be seen in RMSEs of vorticity and temperature predictions against the mesoscale analysis (figures not shown).

To demonstrate the close relationship between axi-symmetric wind field and precipitation distribution, we have prepared Fig. 14 which shows radial distributions of axi-symmetric components of precipitation for Exps. 1A50, 1A20, 1A10, 1B20, and 1D20 by JMA's TYM and by RPN–EC's GEM. TYM and GEM are chosen to exemplify two groups of models featured by different behaviors. Compared to the verifying satellite-estimated profile (thick line), TYM's profiles in Exps. 1A show good

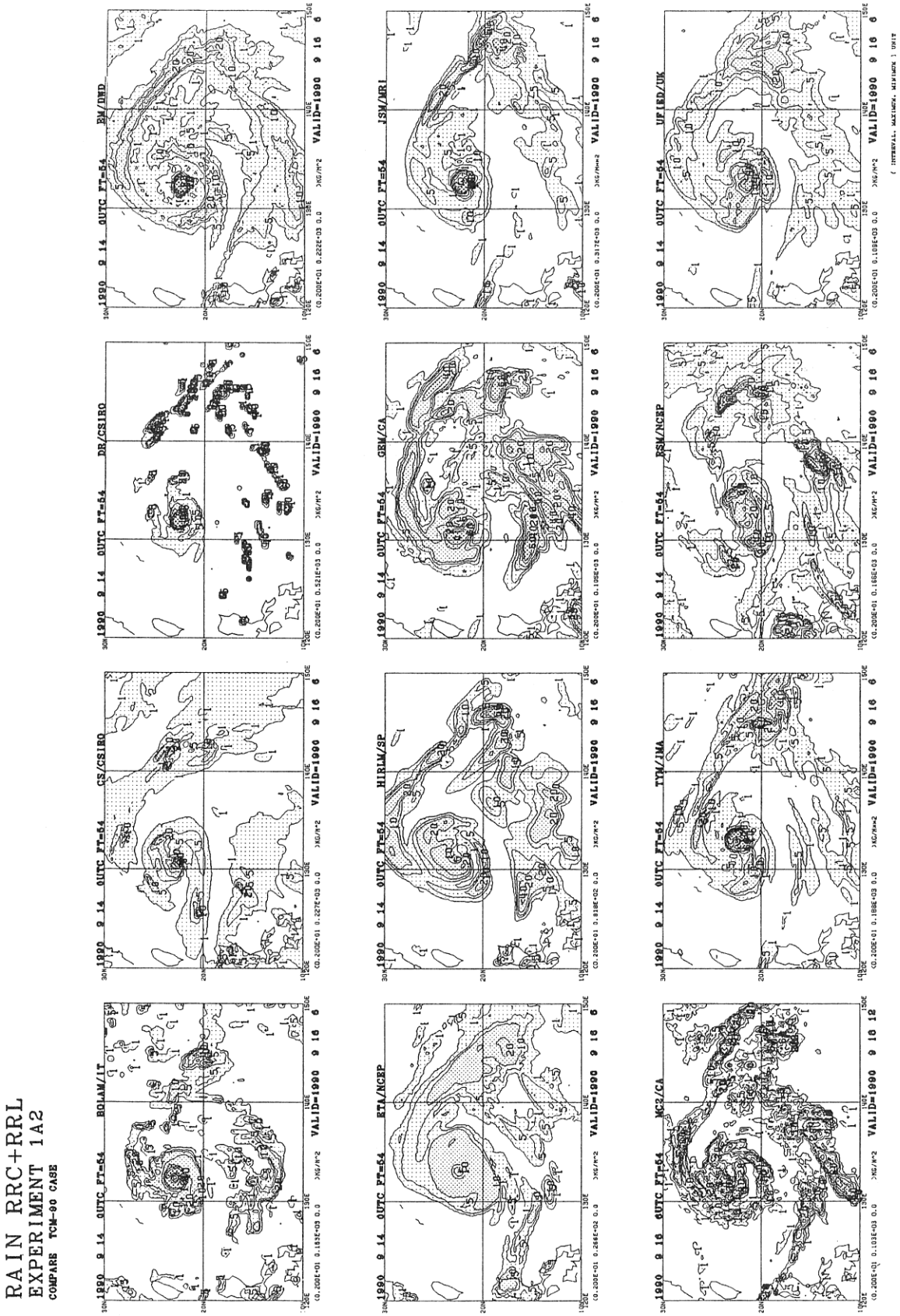

Fig. 12a. Six-hour accumulated total precipitations predicted by models at T+54 h valid at 0600 UTC 16 September 1990 in Exp. 1A20. Contours are 1, 5, 10, 20, 40, 60, ... mm/6 hours.

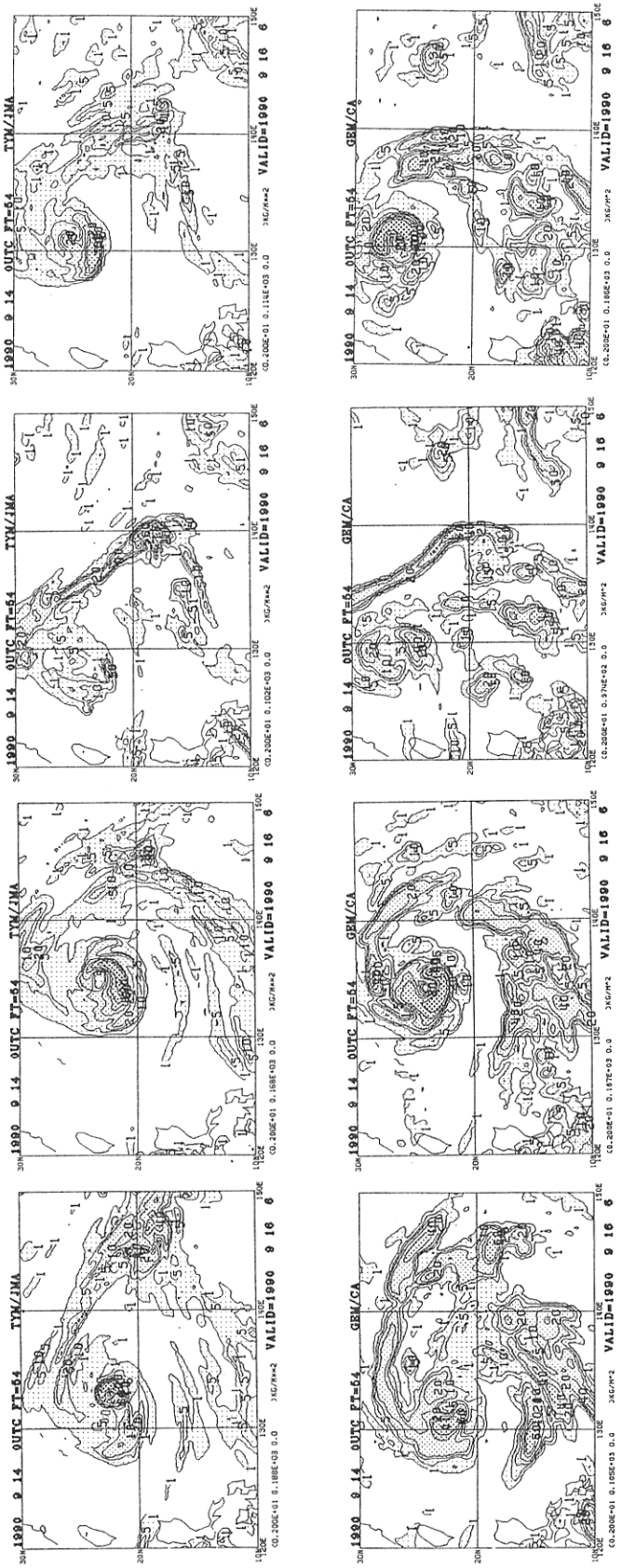

Fig. 12b. Same as Fig. 12a, but for Exp. 1A20, 1B20, 1C20, and 1D20 by JMA's TYM (top) and RPN–EC's GEM (bottom). TYM and GEM are chosen to exemplify two groups of models featured by different behaviors.

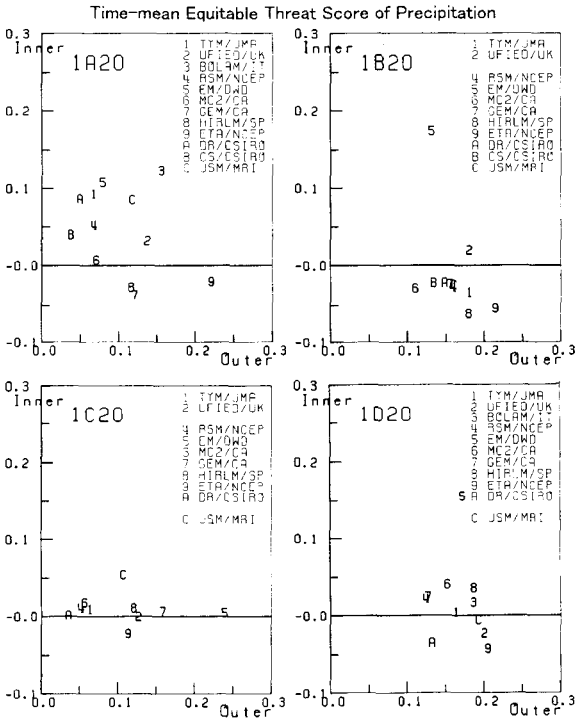

Fig. 13. Scatter plot of time-mean equitable threat scores of total precipitation against the satellite-estimated convective precipitation with a threshold of 10 mm $(6\,\mathrm{h})^{-1}$ between in the inner-core region ($r <$ 200 km, vertical) vs. in the outer region (200 km $\leq r <$ 700 km, horizontal) in the 20-km resolution experiments.

predictions in the inner-core region ($r <$ 200 km) especially in higher resolutions, while increasingly deteriorating predictions in the outer region (200 km $\leq r <$ 700 km) with enhancing resolution. In contrast, TYM in Exps. 1B20 and 1D20 obviously underestimates precipitation in the inner-core region while it simulates precipitation with some skills in the outer region at least for axi-symmetric components. It is natural to speculate that this contrast in precipitation is closely linked to the contrast in wind distribution which has been shown in sub-section 5.1. RPN–EC's GEM produces quite different profiles from those of TYM: concentration of precipitation in the inner-core region with enhanced horizontal resolution is modest in Exps. 1As, while it produces fairly good axi-symmetric components of precipitation in the outer region in most of the experiments. Note here that Fig. 14 compares only axi-symmetric components of precipitation and does not include asymmetric components, both of which in total form are evaluated in Fig. 13.

Another mesoscale evaluation is conducted by verifying upper mesoscale fields against a mesoscale analysis made on a $0.5° \times 0.5°$ grid at 200 hPa valid for 0600 UTC 16 September 1990 (Fig. 15). The temperature and wind analysis (top panel) is based on the NASA DC–8 aircraft observations (Fig. 3). The analysis shows a distinct warm core of 5-K temperature anomaly with a compact cyclonic circulation, even though the magnitude of temperature anomaly might be underestimated due to the modest resolutions of the observational data and the analysis. Such a feature is well reproduced in Exp. 1A20 by the models (ISAO(FISBAT)'s BOLAM, DWD's EM10M, JMA's TYM, MRI's JSM) which show better evolutions of the typhoon's central pressure (Fig. 9). By contrast the models which fail in the simulation of the characteristic evolution of the typhoon's central pressure do not either reproduce well the upper-level mesoscale features. This correlation suggests that accuracy of prediction of a typhoon's intensity change is closely related with the reproducibility of mesoscale structures in the inner core region, which must be reflected in the upper-level mesoscale fields examined here. The same kind of verification is also conducted for temperature and wind fields in Exps. 1B20, 1C20, and 1D20 (figures not shown). To compare the reproducibilities of upper mesoscale fields among the experiments, we make a scatter diagram of Root Mean Square Errors (RMSEs) of vorticity and temperature for a circular region with a radius of 700 km from the typhoon center for each experiment. Figure 16 shows the diagram for Exp. 1A20. It shows that DWD's EM10M and ISAO(FISBAT)'s BOLAM, followed by JMA's TYM in Exp. 1A20, have the smallest combinations of RMSEs, meaning the best reproducibilities of inner-core mesoscale fields in Exp. 1A20. These models are the ones which predict fairly well the characteristic features of the time evolution of central pressure of the typhoon (see Fig. 9 and Table 2).

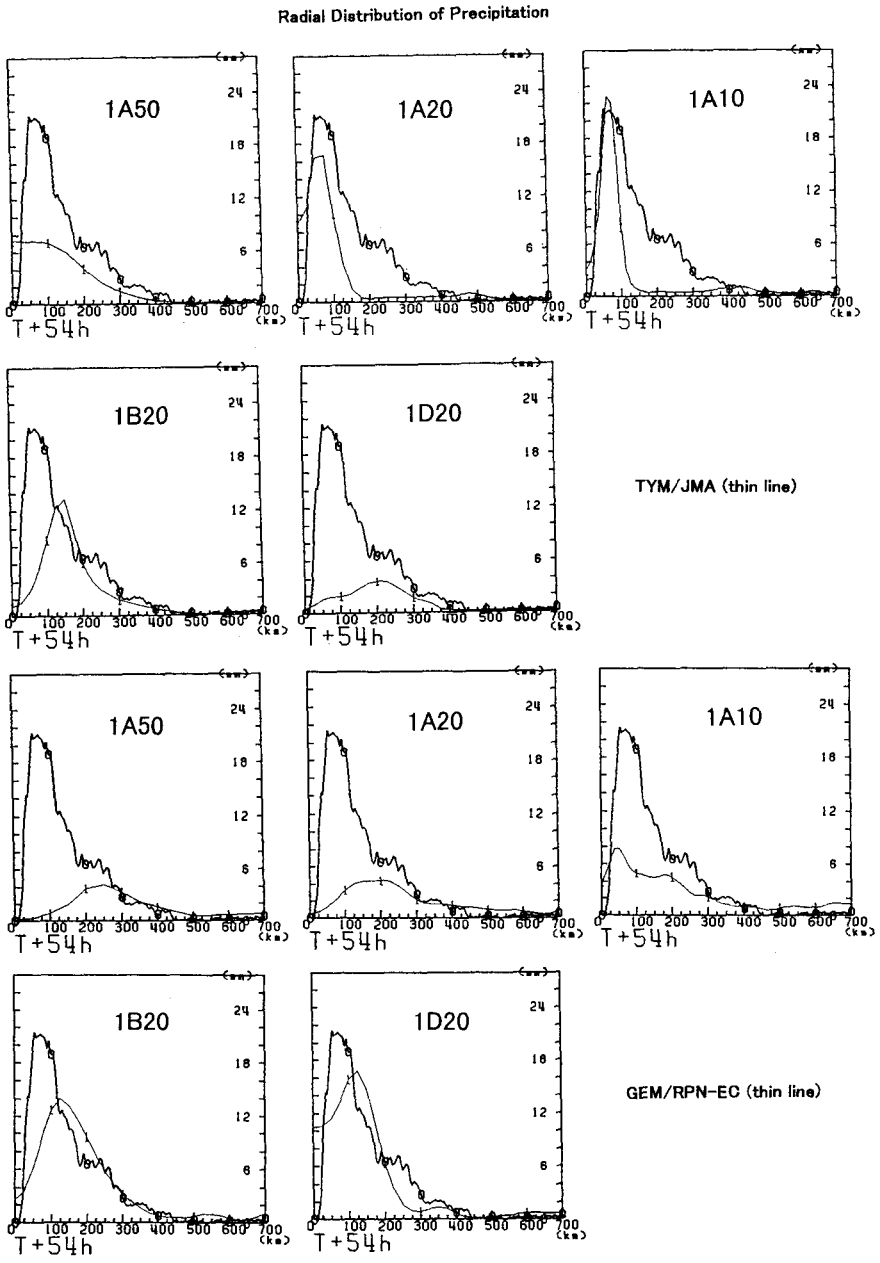

Fig. 14. Radial profiles of axi-symmetric component of total precipitation (thin line) in Exps. 1A50, 1A20, 1A10, 1B20, and 1D20 for JMA's TYM and RPN-EC's GEM in comparison with that of satellite-estimated convective precipitation (thick line). Unit is mm h^{-1}. TYM and GEM are chosen to exemplify two groups of models featured by different behaviors.

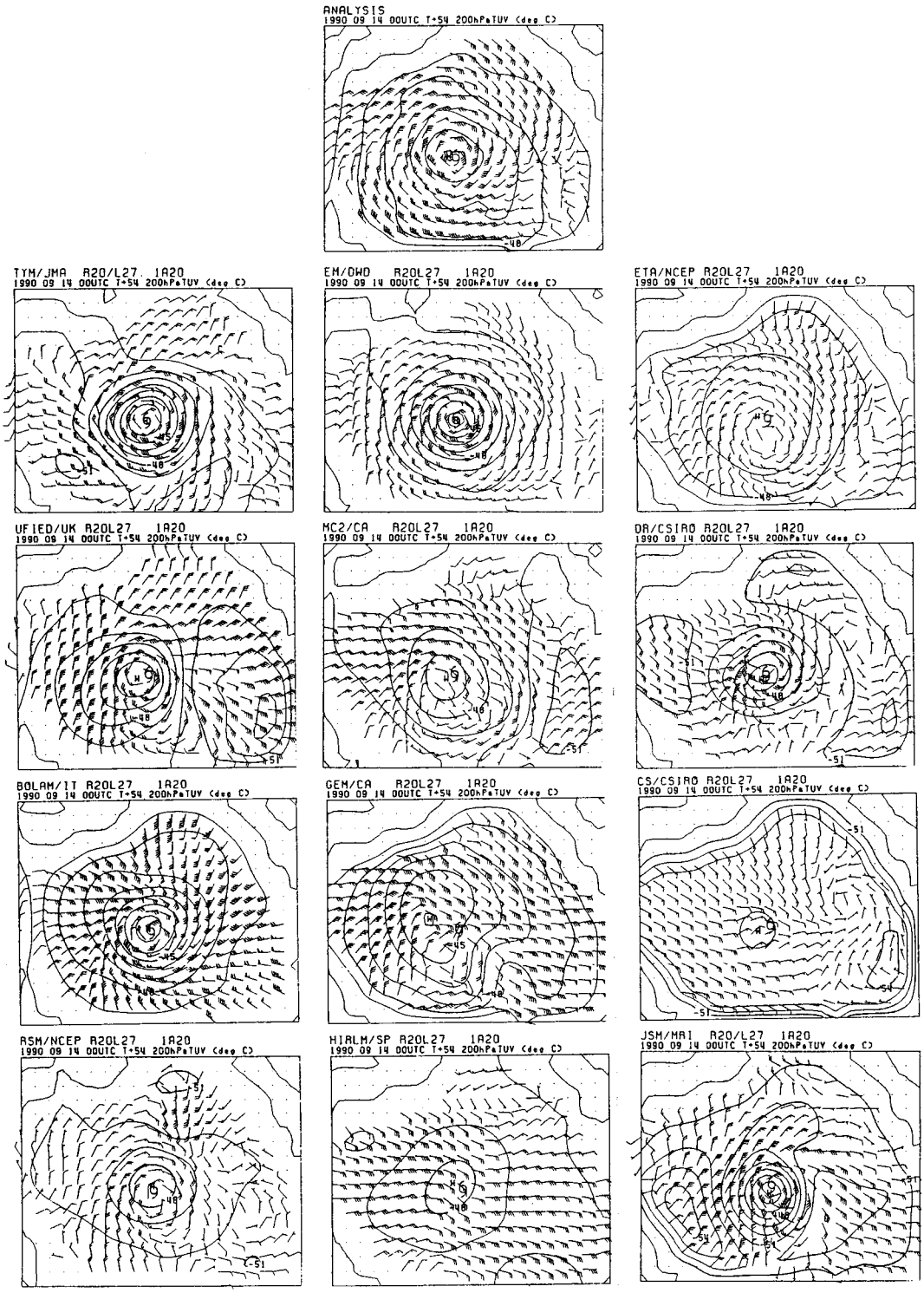

Fig. 15. Objective storm-centered analyses of temperature and wind fields on a 0.5° × 0.5° grid based on NASA/DC-8 observations approximately at 200 hPa with a successive correction method valid for 0600 UTC 16 September 1990 (top panel) and corresponding predictions by the models at T+54 h in Exp. 1A20 (other panels). Contour intervals for temperature are 1 ℃ and wind notation is conventional.

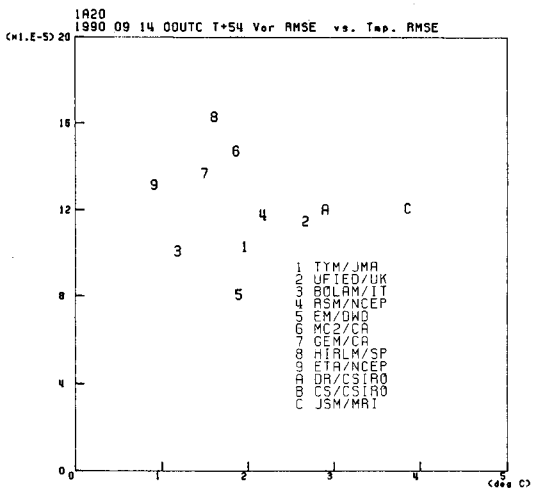

Fig. 16. Scatter plot of scores of upper-level (200 hPa) predicted fields at T+54 h valid at 0600 UTC 16 September 1990 in Exp. 1A20 against objective analysis based on NASA/DC-8 aircraft observations. Root-mean-square (RMS) error of vorticity (vertical) and RMS error of temperature (horizontal) are calculated for a circular region with a radius of 700 km from the typhoon center.

5.4 *Vertical profiles of diabatic heatings and moistenings by moist physics*

At the end of this section, we compare vertical profiles of diabatic heatings and moistenings by moist physical processes; grid-scale condensation/evaporation and cumulus convection among the models for Exps. 1A20, 1B20, and 1D20 (Fig. 17). Averaging is made for the 6-hour time window ending at T+54 h, separately for the inner-core region within the radius of 200 km from the typhoon center and for the outer region with radii greater than 200 km. In the figure we see that even the column integral and vertical profile of the sum of the heatings by the two moist physical processes vary greatly from model to model and among the experiments. The partition of heating between the grid-scale and the convective varies much as well: most heating occurs in grid scale in the inner-core region in some models, while most heating occurs in convection in another group of models. And heating is partitioned approximately evenly between the grid scale and convection in the some other models.

One important finding is that those models which predict fairly well the characteristic features of the time evolution of central pressure of the typhoon in Exp. 1A (DWD's EM10M, ISAO(FISBAT)'s BOLAM, JMA's TYM and MRI's JSM) (see Fig. 9 and Table 2) show very large differences in the heating profiles between the inner and the outer region. The large spatial contrasts in heating must have created intense warm cores and secondary (vertical) circulations in the storm scale leading to strong cyclonic (horizontal) circulations in the low levels balanced with large sea-level pressure gradients through the mass and momentum adjustment process. On the basis of this speculation, realistic simulation of heating amounts, especially that of their spatial contrast between the inner-core and the outer region of TC, is very important for realistic simulation of TC's central pressure evolution. However, the partition of heating between the grid-scale and the convective varies significantly among the four models just mentioned above, which means that the partition is less important in the simulation of TC development than the total heating amount.

It is also noted that models using the Kuo scheme for cumulus convection, such as RPN–MC2 and RPN–GEM, tend to produce most of the heating in convection even in the inner-core region, where the other models tend to have larger ratios of grid-scale heating than in the outer region. However, no particular cumulus parameterization scheme has shown its superiority to the other various schemes in the simulation of TC development in this intercomparison study, in which differences in other factors, such as planetary boundary layer (PBL) scheme, are also involved.

There is another outstanding feature found in Fig. 17. DWD–EM10M shows a unique vertical profile of heating with its maximum at an abnormally low level around 800 hPa in Exp. 1D20. Levels of maximum heating are much higher in the other models or in the other experiments. This unique heating profile of EM10M might explain the excessive deepening seen in the simulation by EM10M in Exp. 1D20 (see Fig. 9).

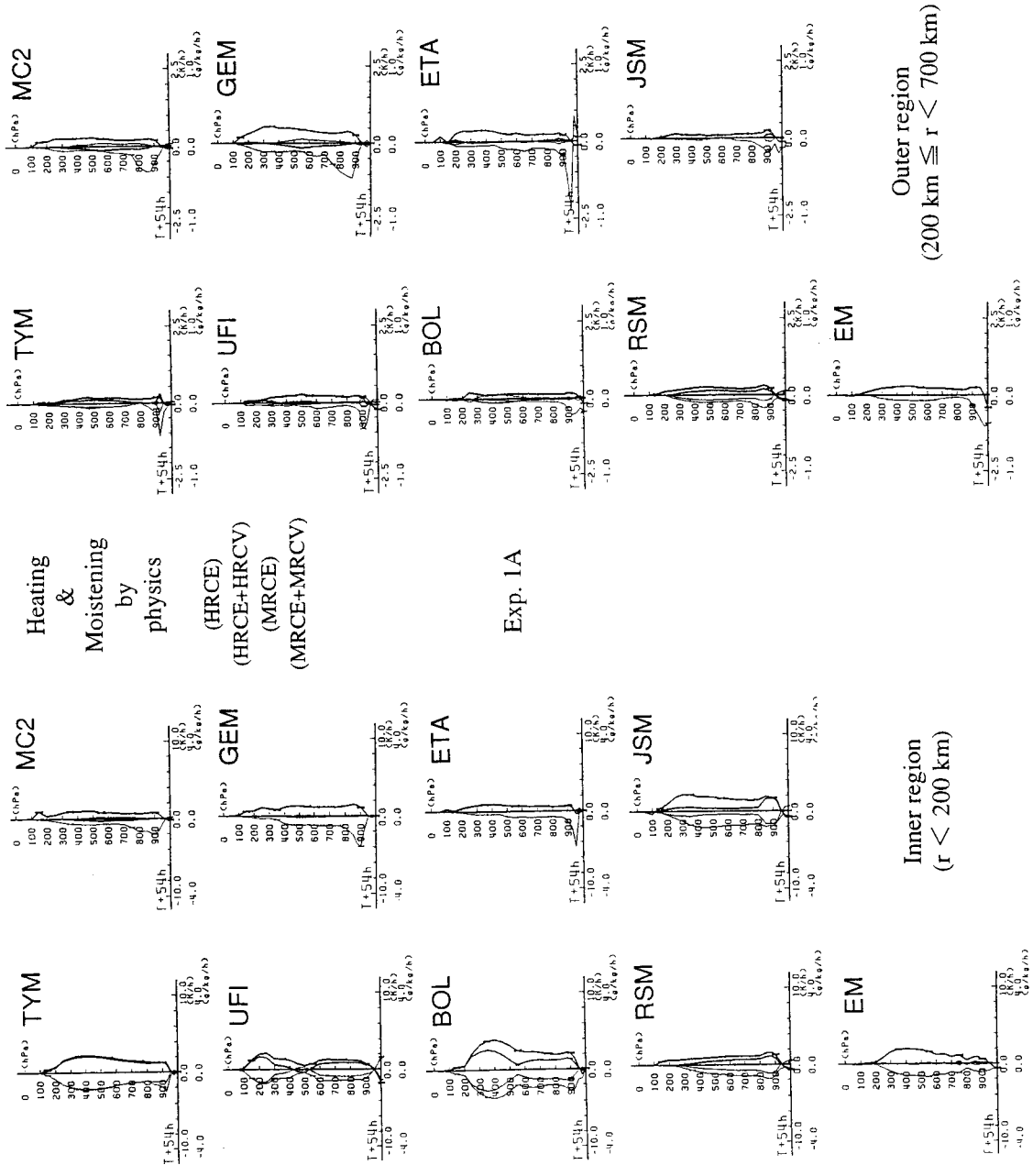

Fig. 17. Vertical profiles of diabatic heatings and moistenings averaged in the inner region ($r < 200$ km, left two columns) and the outer region (200 km $\leq r < 700$ km, right two columns), respectively, for Exps. 1A20, 1B20, and 1D20. Grid-scale condensation and evaporation heating/cooling (HRCE), sum of HRCE and cumulus convective heating (HRCV) and corresponding moistenings (MRCE, MRCV) averaged for 6 h ending at T+54 h (0600 UTC 16 September 1990) are shown. Note that the heating/moistening scales are 4.0 times larger in the inner region than in the outer region.

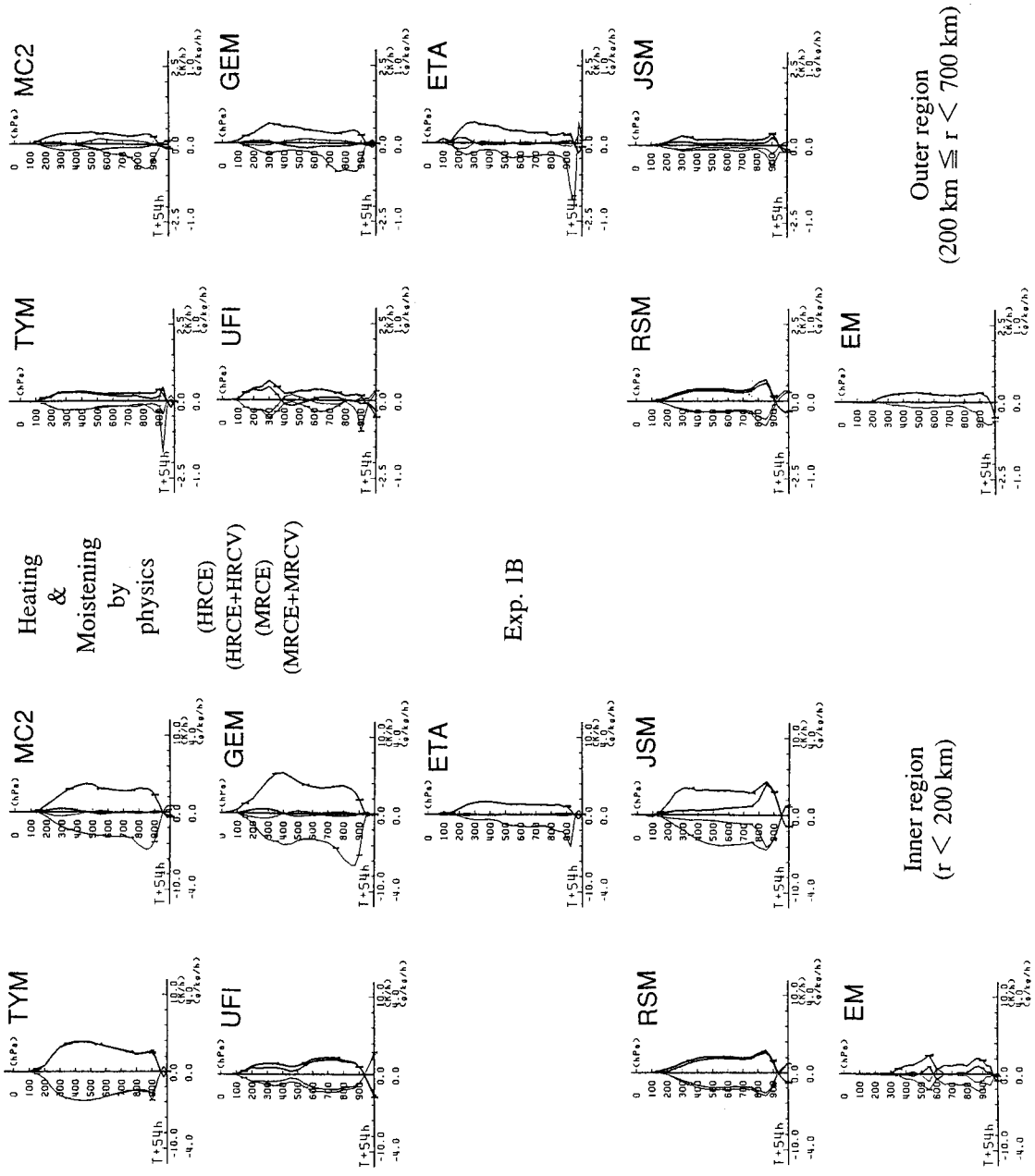
MC2
GEM
ETA
JSM
Outer region
(200 km ≦ r < 700 km)
TYM
UFI
RSM
EM
Heating
&
Moistening
by
physics
(HRCE)
(HRCE+HRCV)
(MRCE)
(MRCE+MRCV)
Exp. 1B
MC2
GEM
ETA
JSM
Inner region
(r < 200 km)
TYM
UFI
RSM
EM

Fig. 17. (cont'd)

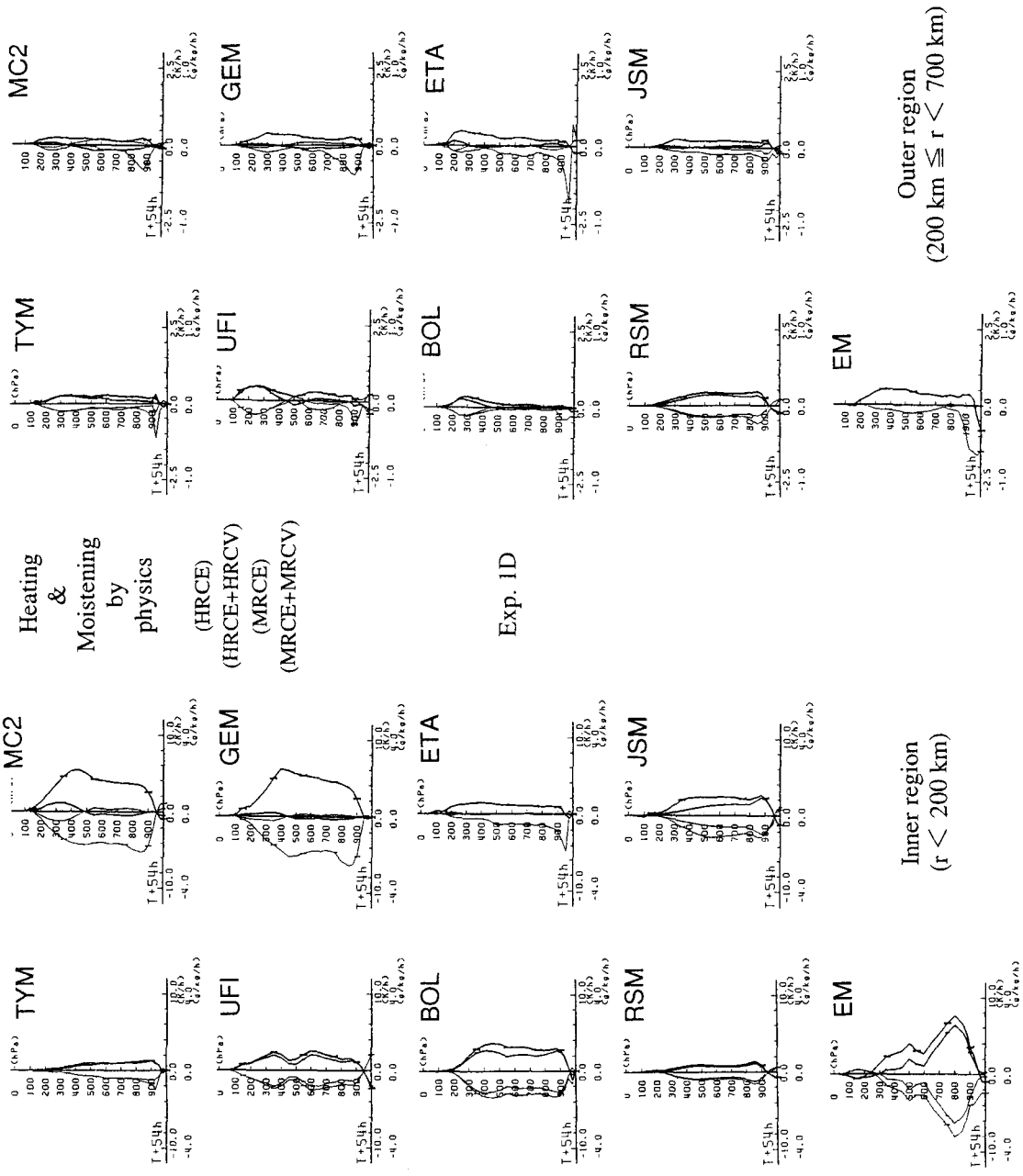
MC2
GEM
ETA
JSM
Outer region
(200 km ≦ r < 700 km)
TYM
UFI
BOL
RSM
EM
Heating
&
Moistening
by
physics
(HRCE)
(HRCE+HRCV)
(MRCE)
(MRCE+MRCV)
Exp. 1D
MC2
GEM
ETA
JSM
Inner region
(r < 200 km)
TYM
UFI
BOL
RSM
EM

Fig. 17. (cont'd)

6. Discussion

In this section some discussion is made about tropical cyclone intensity and its prediction. There have been some observational and theoretical studies investigating maximum potential intensity of tropical cyclones at given sea-surface temperatures (SSTs) (Miller 1958; Merill 1987; Emanuel 1988). Besides this type of "single-cell" thermodynamic explanation, additional pressure drop from subsidence in the eye is pointed out as another factor accounting for very low central pressures (Yamasaki 1983), such as 890 hPa in the case of Flo examined in this study. In these intercomparison experiments, some models show marginal capability of reproducing some subsidence in the eye even with the 20 km horizontal resolution (figures not shown). However, it is obviously insufficient to realistically simulate the eye with the horizontal scale of a few tens of kilometers. Further enhancement of resolution is desirable at least for this reason.

The success of qualitative prediction of intensity change by some numerical models is noted in this case. This might partly be based on the fact that tropical cyclones develop nearly in the same way in the energy budget sense throughout a wide range of horizontal resolutions of numerical models (Tuleya and Kurihara 1975; Bender and Kurihara 1983).

Another significant factor which must have been involved in the intensity change of tropical cyclones, but has not yet been incorporated into the participating models is the coupling of the atmosphere with the ocean. There have been several studies showing significant effects of the coupling on the intensity of tropical cyclones (Bender et al. 1993a; Falcovich et al. 1995; Ginis et al. 1997; Bender and Ginis 2000). They predict more or less weaker storms compared to those in the uncoupled atmosphere. We should take into account this negative impact to intensifying tropical cyclones when we evaluate the performance of the participating models in this case.

7. Summary

In this, the third case of the WMO numerical model intercomparison project COMPARE, the explosive development stage of the tropical cyclone (Typhoon Flo, 9019) is simulated by the fourteen participating models, and evaluated against the available data and analyses from the coordinated field experiments. Focus has been placed on the sensitivity to initial condition as well as the impact of enhanced horizontal resolution. The results show that both track and intensity predictions are very sensitive to the choice of analysis and synthetic tropical cyclone vortex for the initial field. Horizontal resolution enhanced from 50 km through 20 km down to a 10 km grid has a large impact on intensity prediction, presumably due to a better presentation of inner structure with higher resolution, but not on track prediction in this particular case where the typhoon was in its before-recurvature stage.

While most models show large positive biases in central pressure, some of the participating models with a particular initial field have succeeded in reproducing qualitatively the time evolution of central pressure, including the slow deepening in the first half, and the rapid deepening in the second half of the simulation period of 72 hours. However, differences leading to different intensity predictions among models have yet to be identified. Extensive analysis and research is needed to elucidate the differences. To facilitate studies on this and related themes, the COMPARE Steering Committee has decided to establish a data center for an extension of COMPARE III where all the analysis and simulation data are archived on a server workstation. The archive is under construction.

Those models succeeding in qualitatively reproducing the central pressure evolution have realistic concentrations of precipitation in the core region, but systematically small amounts of precipitation in outer regions, resulting in too small sizes in terms of 50 kt and 30 kt wind radii. Meanwhile some of the other models show less concentrations of precipitation in the core region and realistic amounts of precipitation in outer regions, which lead to unacceptable small central pressure deficits but good predictions of the size of the storm defined with the wind radii. Thus, the wind distribution has close relationship with precipitation distribution. This finding suggests that better prediction of precipitation distribution is crucial for better prediction of wind distribution, and vice versa.

Through the COMPARE III experiments, it has become clear that precise simulation of tropical cyclone structure, especially in the inner-core and region, is very important for accurate intensity prediction. Consideration, therefore, should be given to this point, when improvements in resolution, initialization, and physics of numerical models for tropical cyclone intensity prediction are reviewed.

Acknowledgments

The European Centre for Medium-range Weather Forecast (ECMWF) provided the TOVS 1D–VAR Retrieval Data and gave JMA permission to use them in making the reanalysis dataset with the JMA Global Data Assimilation System. Rex Gibson at ECMWF kindly helped JMA staff with processing the data. It is highly appreciated that the GFDL Hurricane Modeling Group, including Robert Tuleya and Morris Bender, voluntarily processed the two sets of analysis data by implanting synthetic tropical cyclones with its sophisticated scheme of tropical cyclone initialization. Toshiyuki Kurino at the Meteorological Satellite Center, JMA Kiyose produced estimates of precipitation based on GMS–IV satellite infrared data and provided them to the authors, which are crucial for evaluation of simulations of precipitation. Kenji Hatano at JMA provided great help in encoding and decoding GRIB-format data.

Thanks are extended to Francois Lalaurette at ECMWF, Andrew Staniforth at RPN/EC (now at UKMO), Joe Klemp at NCAR, Ming Xue at University of Oklahoma, and Peter Clark at Joint Center for Mesoscale Meteorology, UK for their valuable suggestions and advice in the COMPARE Steering Committee and to Mitsuru Ueno at MRI/JMA, Johnny Chan at City University of Hong Kong, and Robert F. Abbey, Jr. at Office of Naval Research, USA for their helpful comments and encouragement. Masanori Yamasaki at the University of Tokyo provided ideas making firm basis for interpretation of the simulations.

This study has been funded by WMO–CAS/JSC WGNE, the Japan Meteorological Agency (JMA), and Japan Science and Technology Agency (STA) and supported by the Meteorological Society of Japan (MSJ).

Appendix A
Participating models

The eleven participating institutions and fourteen models are listed in Table A1. They include the JMA Typhoon Model (TYM; JMA 1997), the United Kingdom Meteorological Office (UKMO) Unified Model (Cullen 1993; Cullen and Davies 1991), the Italian National Research Council Institute of Atmospheric and Oceanic Sciences (ISAO–CNR, formerly FISBAT–CNR) Limited Area Model (BOLAM; Malguzzi and Tartaglione 1999; Buzzi et al. 1994), the National Centers for Environmental Prediction (NCEP) Regional Spectral Model (RSM; Juang and Kanamitsu 1994; Juang et al. 1997), the Deutscher Wetterdienst (DWD) European Model (EM10M; Majewski 1991), the Canadian Atmospheric Environment Service (AES) Recherche en Prévision Numérique (RPN) non-hydrostatic Mesoscale Compressible Community Model (MC2; Benoit et al. 1997; Tanguay et al. 1990; Laprise et al. 1997), the AES RPN Global Environmental Multi-scale Model (GEM; Cote et al. 1998a, b), the Spanish Meteorological Institute (INM) High Resolution Limited Area Model (HIRLAM; Gustafsson and McDonald 1996), the NCEP step-mountain Eta-coordinate Model (Eta; Mesinger et al. 1988), the Commonwealth Scientific and Industrial Research Organisation (CSIRO) Department of Atmospheric Research (DAR) Limited Area Model (DARLAM; McGregor 1993; McGregor et al. 1993), the CSIRO stretched conformal cubic model (CSIRO–S; McGregor, 1996; McGregor and Dix 1998; McGregor and Katzfey 1998), the Meteorological Research Institute (MRI) of JMA Japan Spectral Model (JSM; Segami et al. 1989), the United States Naval Research Laboratory (NRL) Coupled Ocean/Atmosphere Mesoscale Prediction System (COAMPS; Hodur 1997), and the Indian National Centre for Medium Range Weather Forecasting Regional Spectral Model (RSM; Kalnay et al. 1988; Juang and Kanamitsu 1994). The AES RPN MC2 and the NRL COAMPS are non-hydrostatic while the others are hydrostatic models. The JMA TYM, NCEP RSM, INM HIRLAM, MRI/JMA JSM, and NCMRWF RSM are spectral while the others are grid-point models.

Table A1. Specifications of numerical models participating in Case III of COMPARE.

ID #	Institution	Model	Dynamics					
			Domain Map proj.	Equation	Grid	Resolution Horizontal	Vertical (in PBL) lowest at	Time integration
1	JMA (Japan)	TYM (RSM)	regional Mercator	hydrostatic	145x121 257x217	50 km 20 km	27 (9) 996.25 hPa	semi-implicit
2	UKMO (UK)	Unified Model	regional lat-lon	hydrostatic	160x110 280x220	.4425 deg .18 deg	27 (11) 996.25 hPa	foreward/ backward
3	FISBAT (Italy)	BOLAM	regional rot. lat-lon	hydrostatic	132x90 210x170	.48 deg .2 deg	27 (9) / 996 27 (7) / 997 996.0 hPa	foreward- backward
4	NCEP (USA)	RSM	regional Mercator	hydrostatic	145x122 257x218	50 km 20 km	27 (9) 995.0 hPa	semi-implicit
5	DWD (Germany)	EM10M	regional lat-lon	hydrostatic	145x109 201x151	.5 deg .25 deg	27 (9) 996.25 hPa	semi-implicit
6	RPN/EC (Canada)	MC2	regional Mercator	non-hydrostatic	144x120 256x216	50 km 20 km	29 (11) 36.6m/17.8m	semi-implicit
7	RPN/EC (Canada)	GEM	global stretched rot. lat-lon	hydrostatic	178x198 392x480	.5 deg .182 deg variable	29 (11) 997.5 hPa	semi-implicit
8	INM (Spain)	HIRLAM	regional rot. lat-lon	hydrostatic	146x110 252x194	47 km 22 km	27 996.25 hPa	semi-implicit
9	NCEP (USA)	Eta	regional rot. spheric	hydrostatic	145x175 151x305	50 km 20 km	27 (10) 10m	foreward- backward
A	CSIRO (Australia)	DARLAM	regional Mercator	hydrostatic	145x121 257x217	50 km 20 km	27 (9) 996.25 hPa	semi-implicit
B	CSIRO (Australia)	CSIRO-S	global stretched conformal cubic	hydrostatic	154x154 385x385	50 km 20 km	27 (9) 996.25 hPa	semi-implicit
C	MRI/JMA (Japan)	JSM	regional Mercator	hydrostatic	145x121 257x217	50 km 20 km	27 (9) 996.25 hPa	semi-implicit
D	NRL (USA)	COAMPS	regional Mercator	non-hydrostatic	91x91 100x100	50 km 20 km	30 (10) 10m	h: spl.-expl. v: spl.-impl.
E	NCMRWF (India)	RSM	regional Mercator	hydrostatic	97x84	50 km	18 (4) 995 hPa	semi-implicit

Table A1. (cont'd)

ID #	Institution	Model	Physics				Initialization	10-km run
			Horizontal diffusion	Cumulus convection	Grid-scale condens,	Vertical diffusion PBL surface layer		
1	JMA (Japan)	TYM (RSM)	4th-order	Arakawa-Schuber with downdraft and evaporation	Instant precip. with evaporation of rain	Mellor-Yamada level 2.0 similarity theory	diabatic NNMI	yes
2	UKMO (UK)	Unified Model	4th-order	Gregory-Rowntree with downdraft	explicit (Rc, Ri)	K-theory with non-local transp. similarity theory	none	yes
3	FISBAT (Italy)	BOLAM	4th-order	Kain-Fritsch with downdraft	explicit (Rc, Ri, Rr, Rs, Rg)	K-theory depend. on Ri and Z/Z0 K-theory (Louis)	none	yes
4	NCEP (USA)	RSM	4th-order	Arakawa-Schuber with downdraft	Instant precip. with evaporation of rain	K-theory with non-local transp. similarity theory	none	
5	DWD (Germany)	EM10M	4th-order	mass flux with downdraft and evaporation	parameterized microphysics	Mellor-Yamada level 2.0 similarity theory	implicit NNMI	
6	RPN/EC (Canada)	MC2	2nd-order	Kuo (1974) with evaporation	Sundqvist (1978)	TKE prediction similarity theory	dynamic	yes
7	RPN/EC (Canada)	GEM	2nd-order	Kuo (1974) with evaporation	Sundqvist (1978)	TKE prediction similarity theory	digital filter	yes
8	INM (Spain)	HIRLAM	4th-order	Kuo (1974) with evaporation	Sundqvist (1978)	K-theory with non-local transp. similarity theory	none	
9	NCEP (USA)	Eta	non-linear	Betts-Miller-Janjic with evaporation	Sundqvist (1978) Zhao (1997)	Mellor-Yamada level 2.5 similarity theory	Lynch filter (only 20-km run)	
A	CSIRO (Australia)	DARLAM	non-linear	mass flux	Instant precip. with evaporation of rain	K-theory (Louis) similarity theory	none	
B	CSIRO (Australia)	CSIRO-S	non-linear	mass flux with evaporation	Instant precip. with evaporation of rain	K-theory (Louis) similarity theory	none	
C	MRI/JMA (Japan)	JSM	4th-order	Arakawa-Schuber with downdraft and evaporation	Instant precip. with evaporation of rain	Mellor-Yamada level 2.0 similarity theory	diabatic NNMI	yes
D	NRL (USA)	COAMPS	4th-order	Kain-Fritsch with downdraft	Explicit (Rc, Ri, Rr, Rs)	TKE prediction similarity theory	variational balance	
E	NCMRWF (India)	RSM	2nd-order	Kuo (1974) with evaporation	Instant precip. with evaporation of rain	K-theory similarity theory	none	

Appendix B

Table A2. Biases and standard deviations of differences from the first guess in sea-level pressure at drifting buoys.

call sign	name	bias (hPa)	S. D. (hPa)	number of samples
52523	EBEBC	1.8	1.1	113
52525	BEBBE	4.8	1.1	87
52527	EBEBG	6.0	1.0	92
52526	EBEBF	5.8	3.3	109
52530	EBECJ	no report	no report	0
52521	EBEBA	6.2	1.9	110
52522	EBEBB	5.1	1.1	92
52501	EBEJA	2.0	1.8	58
52502	EBEJB	-3.5	2.0	111
52503	EBEJC	-2.7	1.0	69
52504	EBEJD	-0.5	0.7	103

6-hourly (00, 06, 12, 18UTC), 01-30 September 1990

Table A3a. Biases and standard deviations of differences from the first guess in geopotential height at intensive upper-air observation stations in the western North Pacific.

	station	47971 Chichijima	47991 Marcus	91217 Guam	91334 Truk	91348 Ponape	91408 Koror	91413 Yap
	level							
bias (gpm)	850	-3.7	-1.4	-6.1	-2.3	-11.9	-7.2	-11.3
	700	-2.4	0.6	-1.6	2.4	-9.2	-3.1	-5.7
	500	-3.2	-0.6	3.2	8.6	-3.4	4.5	0.6
	400	-4.1	-2.5	7.3	16.1	3.8	12.8	6.2
	300	-1.9	-3.2	14.8	25.9	17.4	14.9	14.8
	250	-2.7	-1.1	18.7	31.6	26.2	18.5	19.3
	200	-6.1	0.9	25.6	35.9	27.1	23.1	23.9
	150	-8.2	0.9	28.0	41.6	34.2	24.6	27.9
	100	-2.9	-2.8	19.0	34.2	29.1	15.0	20.0
	level							
S. D. (gpm)	850	4.5	5.4	6.2	5.0	5.0	6.1	4.3
	700	6.4	6.3	8.0	4.7	6.0	5.5	5.0
	500	11.7	8.6	9.0	5.4	6.5	12.5	8.2
	400	13.7	10.2	9.1	6.1	7.2	24.6	6.0
	300	18.6	11.5	10.4	8.0	18.5	9.0	5.7
	250	19.5	13.8	11.8	9.2	32.1	9.8	7.3
	200	19.7	15.8	14.0	11.0	14.4	11.8	10.1
	150	15.4	15.6	18.2	17.7	15.1	15.6	11.5
	100	16.3	16.5	20.7	22.4	13.4	19.7	11.4
number of samples		59	58	59	58	59	54	53

12-hourly (00, 12UTC), 01-30 September 1990

Table A3b. Biases and standard deviations of differences from the first guess in geopotential height of observation vessels (the four on the left are former USSR's and the two on the right are JMA's R/Vs).

	ship	EREH	EREI	UHQS	UMAY	JBOA	JCCX
	level						
bias	850	-28.8	-30.0	-16.3	-13.3	-3.0	-3.3
(gpm)	700	-29.4	-32.0	-11.5	-10.4	-0.7	-0.3
	500	-27.8	-33.8	-7.6	-2.7	-2.9	-3.3
	400	-29.0	-29.4	-3.4	3.8	-1.5	-0.4
	300	-18.8	-19.9	2.1	16.0	0.6	4.6
	250	-6.2	-13.6	8.1	23.8	4.1	5.0
	200	6.1	-10.2	15.3	31.4	3.0	7.1
	150	16.4	-9.4	19.7	39.0	2.4	0.5
	100	13.1	-21.5	7.8	33.7	3.5	-1.9
	level						
S. D.	850	7.6	8.8	7.3	7.6	9.2	4.0
(gpm)	700	9.5	10.4	8.4	6.8	9.6	3.1
	500	11.3	15.5	13.2	10.8	10.6	7.4
	400	33.0	17.9	13.7	16.0	9.8	8.6
	300	37.2	19.6	14.3	22.8	8.5	6.3
	250	31.4	21.6	17.4	25.6	9.6	9.3
	200	33.9	26.1	24.0	29.2	11.3	9.6
	150	37.9	30.3	34.3	33.3	13.3	10.6
	100	40.0	33.8	41.7	35.1	14.2	15.2
number of samples		45	51	38	35	26	22

12-hourly (00, 12UTC), 01-30 September 1990

Appendix C
Definition of Equitable Threat Score (ETS)

The equitable threat score (ETS) is defined as

$$\mathrm{ETS} = (X - C)/(X - C + Y + Z),$$

where X is the number of hits (forecast: yes, analysis: yes), Y is the number of misses (forecast: no, analysis: yes), Z is the number of false alarms (forecast: yes, analysis: no), and C is the number of hits by chance, i.e., the expected number of hits in a random forecast, which is equal to

$$(X + Y)(X + Z)/(X + Y + Z + W),$$

where W is the number of negative forecasts having negative events (forecast: no, analysis: no). It may be regarded as a kind of critical success index (CSI), in other words threat score (TS), defined as

$$\mathrm{CSI} = X/(X + Y + Z),$$

which has been modified in such a way that hits by chance are removed. ETS does not increase merely with increasing frequency of events unlike CSI does. Thus, ETS is a skill score which can be used for evaluating the degree of skill of a forecast scheme. ETS is zero and unity for a random and a perfect forecast, respectively, while CSI is a non-zero positive value and unity for a random and a perfect forecast, respectively. For an example of an intermediate situation, in a simple case where a square forecast precipitation area of a km $\times$ a km is displaced by $a/2$ km in one direction with respect to a square actual precipitation area of the same size, both CSI and ETS are approximately 0.33, if hits by chance are negligibly small.

References

Adler, R.F. and A.J. Negri, 1988: A satellite infrared technique to estimate tropical convective and stratiform rainfall. *J. Appl. Meteor.*, **27**, 30-51.

Bender, M.A. and I. Ginis, 2000: Real-case simulations of hurricane-ocean interaction using a high-resolution coupled model: effects on hurricane intensity. *Mon. Wea. Rev.*, **128**, 917-946.

———, ——— and Y. Kurihara, 1993a: Numerical simulation of tropical cyclone-ocean interaction with a high-resolution coupled model. *J. Geophys. Res.*, **98**, 23245-23263.

——— and Y. Kurihara, 1983: The energy budget for the eye and eye wall of a numerically simulated

tropical cyclone. *J. Meteor. Soc. Japan*, **61**, 239–243.

———, R.J. Ross, R.E. Tuleya and Y. Kurihara, 1993b: Improvements in tropical cyclone track and intensity forecasts using the GFDL initialization system. *Mon. Wea. Rev.*, **121**, 2046–2061.

Benoit, R., M. Desgagne, P. Pellerin, S. Pellerin and Y. Chartier, 1997: The Canadian MC2: A semi-Lagrangian, semi-implicit wideband atmospheric model suited for finescale process studies and simulation. *Mon. Wea. Rev.*, **125**, 2382–2415.

Buzzi, A., M. Fantini, P. Malguzzi and F. Nerozzi, 1994: Validation of a limited are model in cases of Mediterranean cyclogenesis: Surface fields and precipitation scores. *Meteor. Atmos. Phys.*, **53**, 137–153.

Chouinard, C., J. Mailhot, H.L. Mitchell, A. Staniforth and R. Hogue, 1994: The Canadian Regional Data Assimilation System: operational and research applications. *Mon. Wea. Rev.*, **122**, 1306–1325.

Cote, J., S. Gravel, A. Methot, A. Patoine, M. Roch and A. Staniforth, 1998: The operational CMC–MRB Global Environmental Multiscale (GEM) Model. Part I : Design considerations and formulation. *Mon. Wea. Rev.*, **126**, 1373–1395.

———, J.-G. Desmarais, S. Gravel, A. Methot, A. Patoine, M. Roch and A. Staniforth, 1998: The operational CMC–MRB Global Environmental Multiscale (GEM) Model. Part II: Results. *Mon. Wea. Rev.*, **126**, 1397–1418.

Cullen, M.J.P., 1993: The unified forecast/climate model. *The Meteorological Magazine*, **122**, No. 1449, 81–94.

——— and T. Davies, 1991: A conservative split-explicit integration scheme with fourth-order horizontal advection. *Quart. J. Roy. Meteor. Soc.*, **117**, 993–1002.

Dvorak, V.F., 1975: Tropical cyclone intensity analysis and forecasting from satellite imagery. *Mon. Wea. Rev.*, **103**, 420–430.

———, 1984: Tropical cyclone intensity analysis using satellite data. NOAA Tech. Rep. NESDIS 11, 47pp.

Elsberry, R.L., 1990: International experiments to study tropical cyclones in the western North Pacific. *Bull. Amer. Meteor. Soc.*, **71**, 1305–1316.

———, 1995: Recent advancements in dynamical tropical cyclone track predictions. *Meteor. Atmos. Phy.*, **56**, 81–99.

———, B.C. Diehl, J.C.-L. Chan, P.A. Harr, G.J. Holland, M. Lander, T. Neta and D. Thom, 1990: ONR Tropical Cyclone Motion Research Initiative: Field Experiment Summary. NPS–MR–91–001, Naval Postgraduate School, Monterey California.

Emanuel, K.A., 1988: The maximum intensity of hurricanes. *J. Atmos. Sci.*, **45**, 1143–1155.

Falcovich, A.I., A.P. Khain and I. Ginis, 1995: The influence of air-sea interaction on the development and motion of a tropical cyclone: Numerical experiments with a triply nested model. *Meteor. Atmos. Phys.*, **55**, 167–184.

Gandin, L.S. and A. Murphy, 1992: Equitable skill scores for categorized forecasts. *Mon. Wea. Rev.*, **120**, 361–370.

Ginis, I., M.A. Bender and Y. Kurihara, 1997: Development of a coupled hurricane-ocean forecast system in the north Atlantic. *Preprints, 22nd Conf. Hurr. Trop. Meteor., Ft. Collins, CO*, Amer. Meteor. Soc. Boston, MA 02108, 443–444.

Gustafsson, N. and A. McDonald, 1996: A comparison of the HIRLAM grid point and spectral semi-Lagrangian models. *Mon. Wea. Rev.*, **124**, 2008–2022.

Gyakum, J.R., M. Carrera, D.-L. Zhang, S. Miller, J. Caveen, R. Benoit, T. Black, A. Buzzi, C. Chouinard, M. Fantini, C. Folloni, J.J. Katzfey, Y.-H. Kuo, F. Lalaurette, S. Low–Nam, J. Mailhot, P. Malguzzi, J.L. McGregor, M. Nakamura, G. Tripoli and C. Wilson, 1996: A regional model intercomparison using a case of explosive oceanic cyclogenesis. *Wea. Forecasting*, **11**, 521–543.

Harr, P.A., T. Neta and R.L. Elsberry, 1991: ONR Tropical Cyclone Motion Research Initiative: Data Users Guide to Observations. NPS–MR–91–002, Naval Postgraduate School, Monterey California.

Hodur, R.M., 1997: The Naval Research Laboratory's Coupled Ocean Atmosphere Mesoscale Prediction System (COAMPS). *Mon. Wea. Rev.*, **125**, 1414–1430.

Japan Meteorological Agency, 1997: Outline of the operational numerical weather prediction at the Japan Meteorological Agency. Appendix to Progress Report on Numerical Weather Prediction. Numerical Prediction Division, Japan Meteorological Agency. March 1997.

Juang, H.-M. H., S.-Y. Hong and M. Kanamitsu, 1997: The NCEP regional spectral model: An update. *Bull. Amer. Meteor. Soc.*, **78**, 2125–2143.

——— and M. Kanamitsu, 1994: The NMC Nested Regional Spectral Model. *Mon. Wea. Rev.*, **122**, 3–26.

Kalnay, E., J.G. Sela, K.A. Campana, B,K. Basu, M.D. Schwarzkopf, P.E. Long, P.M. Caplan, and J.C. Alpert, 1988: Documentation of the Research Version of the NMC Medium Range Forecasting Model. NCEP, Environmental Prediction Centers, USA.

Kurihara, Y., M.A. Bender and R.J. Ross, 1993: An initialization scheme of hurricane models by vortex specification. *Mon. Wea. Rev.*, **121**, 2030–2045.

———, R.E. Tuleya and M.A. Bender, 1998: The

GFDL Hurricane Prediction System and its performance in the 1995 hurricane season. *Mon. Wea. Rev.*, **126**, 1306–1322.

Laprise, R., D. Caya, G. Bergeron and M. Giguere, 1997: The formulation of the Andre Robert MC2 Model. Atmos.-Ocean, Special Vol.XXXV, No.1, 466–475.

Liu, Y., D.-L. Zhang and M.K. Yau, 1997: A multiscale numerical study of Hurricane Andrew (1992). Part I: explicit simulation and verification. *Mon. Wea. Rev.*, **125**, 3073–3093.

Majewski, D., 1991: The EUROPA-model of the Deutscher Wetterdienst. *ECMWF Seminar Proceedings*, Vol.2, Numerical methods in atmospheric models, 147–191.

Malguzzi, P. and N. Tartaglione, 1999: An economical second order advection scheme for numerical weather prediction. *Quart. J. Roy. Meteor. Soc.*, **125**, 2291–2303.

McGregor, J.L., 1993: Economical determination of departure points for semi-Lagrangian models. *Mon. Wea. Rev.*, **121**, 221–230.

———, 1996: Semi-Lagrangian advection on conformal-cubic grids. *Mon. Wea. Rev.*, **124**, 1311–1322.

——— and M.R. Dix, 1998: A conformal-cubic atmospheric general circulation model. In Research Activities in Atmospheric and Oceanic Modelling Report No.27 (ed. A. Staniforth) WMO/TD-No. 865, 322–323.

——— and J.J. Katzfey, 1998: NWP experiments with a variable-resolution conformal-cubic primitive equations model. In Research Activities in Atmospheric and Oceanic Modelling Report No.27 (ed. A. Staniforth) WMO/TD-No.865, 321–321.

———, K,L. Walsh and J.J. Katzfey, 1993: Nested modelling for regional climate studies. Modelling Change in Environmental Systems, A.J. Jakeman, M.B. Beck and M.J. McAleer Eds., Wiley, 367–386.

Merill, R.T., 1987: An experiment in the statistical prediction of tropical cyclone intensity change. 17th Conf. Hurricanes and Tropical Meteorology, Miami, FL, *Amer. Meteor. Soc.*, 302–304.

Mesinger, F. and T.L. Black, 1992: On the impact of forecast accuracy of the step-mountain (eta) vs. sigma coordinate. *Meteor. Atmos. Phys.*, **50**, 47–60.

———, Z.I. Janjic, S. Nickovic, D. Gavrilov and D.G. Deaven, 1988: The step mountain coordinate: Model description and performance for cases of Alpine lee cyclogenesis and for a case of an Appalachian redevelopment. *Mon. Wea. Rev.*, **116**, 1493–1518.

Miller, B.I., 1958: On the maximum intensity of hurricanes. *J. Meteor.*, **15**, 184–195.

Mino, H. and M. Nagata, 2001: Outline of the new typhoon prediction models at JMA. *RSMC Tokyo–Typhoon Center Technical Review*, No.4, 1–13, March 2001.

Nagata, M. and H. Mino, 2000: Intensity prediction of tropical cyclones I : How well does a current dynamical model predict tropical cyclone intensity? *Preprints for the semi-annual meeting of the Meteorological Society of Japan*, **77**, 148. (in Japanese)

———, Y. Tahara and C. Muroi, 1998: Enhanced accuracy of typhoon prediction of the advanced numerical models at the Japan Meteorological Agency. *Tech. Rev., RSMC Tokyo–Typhoon Center*, No.2, 1–18, March 1998.

Rogers, E., T.L. Black, D.G. Deaven, G.J. Dimego, Q. Zhao, M. Baldwin, N.W. Junker and Y. Lin, 1996: Changes to the operational "Early" Eta Analysis/Forecast System at the National Centers for Environmental Prediction. *Wea. Forecasting*, **11**, 391–413.

Schaefer, J,T., 1990: The critical success index as an indicator of warning skill. *Wea. Forecasting*, **5**, 570–575.

Segami, A., K. Kurihara, H. Nakamura, M. Ueno, I. Takano and Y. Tatsumi, 1989: Operational mesoscale weather prediction with Japan Spectral Model. *J. Meteor. Soc. Japan*, **67**, 907–924.

Tanguay, M., A. Robert and R. Laprise, 1990: A semi-implicit semi-Lagrangian fully compressible regional forecast model. *Mon. Wea. Rev.*, **118**, 1970–1980.

Tuleya, R.E. and Y. Kurihara, 1975: The energy and angular momentum budget of a three-dimensional tropical cyclone model. *J. Atmos. Sci.*, **32**, 287–301.

Velden, C.S., T.L. Olander and R.M. Zehr, 1988: Development of an objective scheme to estimate tropical cyclone intensity from digital geostationary satellite infrared imagery. *Wea. Forecasting*, **13**, 172–186

Yamasaki, M., 1983: A further study of the tropical cyclone without parameterizing the effects of cumulus convection. *Pap. Meteor. Geophys.*, **34**, 221–260.

Wu, C.-C., M.A. Bender and Y. Kurihara, 2000: Typhoon forecast with the GFDL Hurricane Model: forecast skill and comparison of predictions using AVN and NOGAPS global analyses. *J. Meteor. Soc. Japan*, **78**, 777–788.